Submitted to Physical Review C

LBL-4368
Preprint

THE $(\alpha, {}^{8}Be)$ REACTION IN THE 1P SHELL

G. J. Wozniak, D. P. Stahel, Joseph Cerny, and
N. A. Jelley

April 1976

Prepared for the U. S. Energy Research and
Development Administration under Contract W-7405-ENG-48

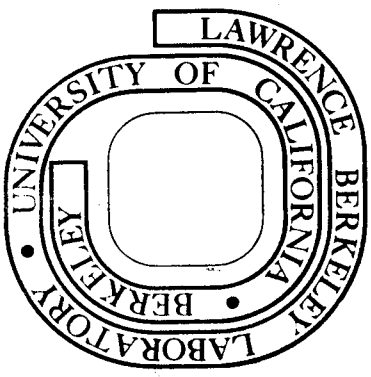

LBL-4368

DISCLAIMER

LBL-4368

THE (α, ^{8}Be) REACTION IN THE 1P SHELL*

G. J. Wozniak, D. P. Stahel and Joseph Cerny

Department of Chemistry and
Lawrence Berkeley Laboratory
University of California
Berkeley, California 94720

and

N. A. Jelley
Nuclear Physics Laboratory
University of Oxford
Oxford, England

April 1976

ABSTRACT

A ^{8}Be identifier of high detection efficiency was utilized to investigate the (α, ^{8}Be) reaction on ^{16}O, ^{15}N, ^{14}N, ^{13}C, ^{12}C, ^{11}B, ^{10}B and ^{9}Be targets at bombarding energies between 65 and 72.5 MeV. Differential cross sections were measured from $\Theta_{c.m.}$ = 20° - 70° for solid targets and over a more restricted range for the nitrogen gas targets. Excitation functions were obtained over a larger energy range for the ^{12}C and ^{16}O targets. At these energies, the (α, ^{8}Be) reaction was found to proceed predominantly via a direct α-cluster pickup mechanism and to populate strongly only those levels consistent with this mechanism. The data were analyzed in the framework of the exact finite-range distorted-wave Born-approximation. Absolute and relative α-particle spectroscopic factors were extracted for 22 states using finite-range DWBA. Good agreement was found between these experimental values and the theoretical predictions of Kurath and of Rotter for the extent of α-clustering in these light nuclei.

[NUCLEAR REACTIONS ^{16}O, ^{15}N, ^{14}N, ^{13}C, ^{12}C, ^{11}B, ^{10}B, ^{9}Be(α, ^{8}Be) E_α = 65 - 72.5 MeV; measured $\sigma(E_f,\Theta)$; energy levels ^{12}C, ^{11}B, ^{10}B, ^{9}Be, ^{8}Be, ^{7}Li, ^{6}Li, ^{5}He; resolution 400 keV; DWBA analysis, deduced S_α for 22 states, comparisons with theoretical S_α.]

I. INTRODUCTION

The existence and the importance of multinucleon correlations in nuclei[1,2], and in particular of α-like four nucleon correlations[3-7], has intrigued physicists for decades. Recently, detailed theoretical calculations have been made of the extent of α-clustering in light nuclei[8,9] and several reactions have been employed to verify experimentally these predictions.[10,11]

Reactions involving the pickup or knockout of an α particle are good probes of such correlations and in particular the $(d,{}^{6}Li)$[12,13], $({}^{3}He,{}^{7}Be)$[14,15] and the $(\alpha,2\alpha)$[16] reactions have been extensively utilized on light nuclei. Because of uncertainties in the parameters of the theoretical models used to describe these reactions, it is difficult to extract absolute α-particle spectroscopic factors (S_α) from the measured cross sections. However, relative spectroscopic factors as well as information on the reaction mechanism have been obtained.

To complement the information acquired with the above three reactions, a very detailed study on 1p shell targets has been made with the $(\alpha,{}^{8}Be)$ reaction. This reaction has an a priori simplicity because the ^{8}Be ground state looks very much like two α particles weakly bound in a relative s-state; further, since the projectile, the transferred α particle and the ^{8}Be ground state all have zero spin, simple selection rules result. Although ^{8}Be is particle-unstable ($t_{1/2} \sim 10^{-16}$s), its ground state is long-lived compared to nuclear transit times, and one should be able to treat it as a single nucleus in a direct reaction. To investigate this sparsely utilized reaction[17,18], a special identifier was developed[19] which detects the particle-unbound ^{8}Be nucleus. Moreover this identifier eliminated from the spectra any contributions from transitions to excited states of ^{8}Be.

The present investigation was carried out at moderately high bombarding energies (65 - 72.5 MeV) where it was hoped that direct processes would dominate and thus make possible the extraction of experimental spectroscopic factors. All stable lp shell targets were investigated and the data were analyzed in the framework of the exact finite-range distorted-wave Born-approximation (EFR-DWBA). In section II the experimental method is described and in section III the experimental results are presented. Absolute and relative S_α were extracted and are compared to theoretical S_α in section IV. Finally, a summary and conclusions are presented in section V.

II. EXPERIMENTAL METHOD

The study of reactions with ^{8}Be nuclei as the detected particles is complicated by the fact that the ^{8}Be ground state decays promptly, and must be observed indirectly by means of its breakup α particles. The essential problem lies in detecting these two particles with high efficiency, while at the same time accurately determining the energy and direction of the original ^{8}Be event.

Detection systems for ^{8}Be reaction products fall into two general categories: those which incorporate kinematic compensation[19] of the energy variation across the ^{8}Be acceptance angle and those which do not.[17,20-26] The latter systems limit this energy spread by using collimators to define the ^{8}Be acceptance angle while the former utilize a position-sensitive-detector (PSD) to measure the ^{8}Be direction and hence permit kinematic compensation. To obtain a large effective geometry, a ^{8}Be detection system must subtend a large solid angle. Hence, methods which rely on collimation cannot simultaneously optimize both the efficiency and the energy resolution for light targets since a small acceptance angle is necessary for small kinematic broadening. However, if a PSD is used to measure both the direction and the energy of a ^{8}Be event, the detection efficiency and the energy resolution may be optimized concurrently with no restriction on the acceptance angle.

A counter-telescope system capable of identifying ^{8}Be events is outlined below; it incorporates a PSD as an E-detector. To obtain selective ^{8}Be identification, a subnanosecond coincidence between twin transmission (ΔE) detectors is employed. This technique permits low cross section reactions ($\gtrsim$ 0.1 μb/sr) to be efficiently studied at high counting rates (50 kcps). The ^{8}Be identifier

described in this paper incorporates a number of simplifying features and a larger effective solid angle (1 msr) than our previously reported design for such a system.[19]

A. ^{8}Be Identifier

The decay of the ^{8}Be ground state is characterized by a single decay channel, a small breakup energy (Q = 0.092 MeV), two identical charged products (α particles) and, since all the spins involved are zero, an isotropic distribution of the decay products in their center of mass. By designing a detection system for high-energy ^{8}Be events [$E(^8Be) \equiv E_8 > 35$ MeV], advantage can be taken of the strong kinematic focusing of the α particles into a narrow breakup cone (apex angle $<6^\circ$) whose axis lies in the direction of the original ^{8}Be event. The distribution of the breakup α particles is sharply peaked at the surface of the breakup cone; thus, in order to detect a substantial fraction of the ^{8}Be events, a detector should subtend an angle larger than the opening angle of the cone. For a large angular acceptance (10°), a considerable variation in the detection angle (θ_{lab}) of the ^{8}Be events is possible. On light targets ($A \leq 16$), a typical value of $dE/d\theta$ near 25° (lab) for the (α,^{8}Be) reaction at $E_\alpha \sim 65$ MeV is around 500 keV/deg. The substantial kinematic broadening that would occur can be compensated for by using a PSD.

A particle striking a position-sensitive-detector generates both an energy signal E, and a signal XE proportional to the product of its energy E and its distance of impact X from one side of the detector; see Fig. 1. For high energy ^{8}Be events, the breakup Q-value is small compared to the ^{8}Be energy, and so the two breakup α particles have, to a good approximation, equal energies. On striking a PSD, one α particle produces a signal $X_1E/2$; the other, $X_2E/2$. Since both α particles arrive within a fraction of a nanosecond of one another, the individual E and XE signals are automatically summed and the resultant E

signal gives the energy of the ^{8}Be event. The position signal X obtained by dividing out the energy dependence is given by:

$$X = (X_1E/2 + X_2E/2)/(E/2 + E/2) = (X_1 + X_2)/2.$$

In addition to having equal energies, the two α particles are detected at approximately equal distances from the axis of the ^{8}Be breakup cone, which corresponds to the direction of the original ^{8}Be event as shown in Fig. 1. Since this average position X establishes the direction[19] of the ^{8}Be event (Θ_{lab}), substantial kinematic broadening can be compensated for by gating the energy signals with position signals corresponding to a small angular range.

While good efficiency and energy resolution can be obtained with a PSD alone, numerous particle-stable nuclei would also be detected and obscure ^{8}Be events except when they happened to be more energetic. To select only ^{8}Be events, a twin transmission detector is placed in front of the PSD as shown in Fig. 1. This detector consists of a single silicon wafer with two ΔE counters diffused side by side.[27] By making a subnanosecond coincidence between these detectors, ^{8}Be events can be selectively observed as shown in Fig. 2a. This fast coincidence not only eliminates particle-stable nuclei, but also eliminates inter-beam-burst chance coincidence events, which, because of the microscopic duty cycle of the cyclotron beam, come ∿ 100 ns apart.

In addition this subnanosecond coincidence also removes a substantial fraction of the intra-beam-burst pileup. When ^{8}Be decays, the two breakup α particles have approximately the same energy and thus their time-of-flight difference (ΔTOF) to the upper and lower ΔE detectors is approximately zero. The full width at the base of the peak in Fig. 2a (2 ΔTOF = 0.85 ns) illustrates the similiar flight times of the two α particles and the central dip is the effect of collimation on their velocity distribution.[19] By performing a

subnanosecond coincidence between the upper and lower halves of the twin ΔE detectors, the intra-beam-burst background can be reduced by a factor of ten, since the typical beam-burst width at the Berkeley 88-inch cyclotron is approximately 5 ns (at a frequency of 9 MHz). Some further reduction in background[28] and additional selection of ^{8}Be events is obtained by performing particle identification with the summed ΔE and E signals as shown in Fig. 2b (^{8}Be identifies as if it were a ^{7}Li event[18]).

Since commercially available PSDs give position information along their longest dimension, the largest effective solid angle and kinematic compensation are obtained by orienting the twin transmission detector as shown in Fig. 1. In this configuration ^{8}Be events can be detected over an angular spread of several degrees with an almost constant detection efficiency. Characteristics of this particular geometry and the other geometries employed in the various experiments are given in Fig. 3 and Table I. Shown in Fig. 3 are the effective solid angles Ω_{eff} for several identifier geometries as a function of the ^{8}Be energy; Table I gives the geometry parameters employed. The effective solid angle decreases at lower energies due to the increasing size of the breakup cone ($\Omega_{eff} = \varepsilon\Omega_{acc}$ where Ω_{acc} is the acceptance solid angle and ε is the detection efficiency: see Ref. 19 for further details).

B. Experimental Procedure

The experiments discussed in this work utilized 55 -72.5 MeV α-particle beams from the Lawrence Berkeley Laboratory 88-inch cyclotron. Intensities of 1 to 2 μA were readily delivered on target. Typical beam spot sizes were 1.5 × 2.0 mm and the beam energy resolution was 0.14%. To deflect low energy electrons, an 800 G permanent magnet was placed in front of the ^{8}Be identifier, which was mounted on a platform inside a 0.51 meter scattering chamber.

A pressure of $\sim 4 \times 10^{-5}$ Torr was maintained in this chamber and, to eliminate carbon buildup on the targets, a hollow cylindrical liquid nitrogen cold trap was placed along the beam axis immediately upstream from the target. The detectors were placed close to the target (8 to 13 cm) for good detection efficiency. Because several different versions of the ^{8}Be identifier were employed in the course of these experiments, the effective solid angles varied from 0.15 to 1.3 msr (see Fig. 3 and Table I). An experimental ^{8}Be energy resolution of 400 keV was obtained (important contributions to this arose from the radial width of the beam spot and from the high counting rate (50 kcps)).

Self-supporting ^{9}Be, ^{10}B(98%), ^{11}B(98%), ^{12}C, ^{13}C(90%) and SiO_2 targets were used in these experiments. Table II gives the target thicknesses and the detection geometry employed in the particular measurement. Target thicknesses were determined by placing a thin ^{212}Pb source behind each target and measuring the energy loss of the α particles passing through it. In addition, for targets of natural isotopic composition, a 1 cm^2 central circular portion was punched out and weighed on a microbalance.

A gas target and recovery system was used in the experiments with chemically pure $^{14}N_2$, $^{16}O_2$ and isotopically enriched $^{15}N_2$ (99%) gases at a pressure of 0.3 atm. To define the extent of the gas target from which ^{8}Be events could be observed, a second, more forward collimator was also used.[19] For this two collimator system, the energy dependence of the detection efficiency was estimated using a simple correction to the calculation for a single collimator. Comparisons between data taken with oxygen gas targets and SiO_2 targets were used to normalize the gas target cross sections.

Several surface-barrier position-sensitive-detectors[29] with active areas of 13 × 20, 10 × 30, and 10 × 50 mm^2 and depletion depths ranging from 300 to 500 μm were used. These PSDs all had position resolutions of 0.5% to 1% of their length. Their measured energy resolution was 70 keV FWHM and the observed change in pulse-height across their length was 100 keV for 8.78 MeV α particles.

Fully depleted phosphorus-diffused transmission detectors with depletion depths of 100 to 200 μm and active areas of 80 to 130 mm^2 were fabricated at the Lawrence Berkeley Laboratory. Typically, these detectors gave a good signal-to-noise ratio and held a large voltage gradient (2 V/μm), ensuring fast ($<$ 1 ns) collection of the deposited charge. Subnanosecond timing was possible with these detectors using preamplifiers mounted outside the chamber vacuum and simply connected to the detectors via a 50Ω coaxial cable 40 cm in length. The preamplifiers gave both a fast and a charge-sensitive (slow) output and were similiar to those described in Ref. 19 except that the first stage FET was incorporated in the preamplifier.

As indicated in the block diagram of the electronics for the ^{8}Be identifier shown in Fig. 4, the fast outputs of the ΔE_L and ΔE_U preamplifiers fed two constant-fraction discriminators (CFD), which were connected to a time-to-amplitude converter (TAC). The energy deposited in these ΔE detectors by α particles under our experimental conditions varied between 4 and 11 MeV, but no additional time-walk-with-amplitude compensation was required for good time resolution, since ^{8}Be events generate ΔE_L and ΔE_U signals of approximately equal amplitude. Pileup rejectors (PUR) on all three detectors eliminated inter-beam-burst chance-coincident events. A simulated 40 MeV ^{8}Be event gave a time resolution of 200 ps FWHM. Particle identification PI, position X and time-of-flight ΔTOF gates were set with single channel analyzers (SCAs); energy spectra, gated by these parameters, and routed

by position were collected on a 4096 channel analyzer. Gated PI, position and ΔTOF spectra were monitored during the experiments. Dead times were measured by comparing the number of pulser events (triggered by a monitor counter) in the spectrum to the number of pulser triggers.

During an experiment, energy spectra routed by up to four position gates were accumulated in 1024 channel groups of the multichannel analyzer. At the end of a run these data were transferred to an SCC-660 computer and written on magnetic tape. Upon completion of an experiment, analysis of these energy spectra was performed with an interactive, Gaussian peak-fitting program. The detection efficiency and effective solid angle for a ^{8}Be event were calculated with the program EFFCR.[30]

III. RESULTS

In analogy to the analysis of direct single-nucleon pickup reactions, one hopes that the main features of the four-nucleon pickup reaction (α, ^{8}Be) can be understood by assuming that the four nucleons are transferred as a single cluster having the internal quantum numbers of a free α particle. For the nucleus B $\rightarrow$ A + α, the harmonic oscillator quantum numbers NL_α describing the motion of the α cluster with respect to the core A are given by the relation (assuming that the internal quantum numbers of the cluster are zero)

$$2(N-1) + L_\alpha = \sum_{i=1}^{4} [2(n_i - 1) + \ell_i] \qquad (1)$$

where $n_i \ell_i$ are the shell model quantum numbers of the 2 protons and 2 neutrons which form the cluster. Thus, for α clusters in the 1p shell, the values of NL_α are restricted to 3S, 2D and 1G.

Since the projectile, the outgoing ^{8}Be (treated as two α particles in a relative s-state) and the transferred cluster all have zero spin, quite restricted selection rules apply to the assumed simple direct reaction B(α, ^{8}Be)A: for total angular momentum transfer $\vec{J}$ and orbital angular momentum transfer $\vec{L}$

$$\vec{J} = \vec{L} = \vec{J}_B - \vec{J}_A = \vec{L}_\alpha; \qquad \Delta\pi = (-1)^L \tag{2}$$

where $\vec{L}_\alpha$ is the orbital angular momentum of an α cluster in the target nucleus B. In addition the isospin change is given by $\Delta T = 0$. Thus for target nuclei having ground state spins of 0 or 1/2, the transferred angular momentum L has a unique value for transitions to any final state. A summary of all the low excitation final states which possibly could be populated by the (α, ^{8}Be) reaction in the 1p shell is presented in Table III.[31,32] Measured excitation energies and peak cross sections are given and, where determined, upper limits are indicated for very weakly populated states. The theoretical spectroscopic factors[8,9] are also tabulated. If a final state can be populated by several different orbital angular momentum transfers, the sum $S = \sum_{L_\alpha} S^{L_\alpha}$ is given. All final states populated by the (α, ^{8}Be) reaction will be discussed below. The measured angular distributions will be presented with only statistical error bars on the data points; this indicates the relative error although the absolute cross sections could be in error by as much as 30%. Section IV discusses the fitting of the experimental angular distributions.

A. ^{16}O(α, ^{8}Be)^{12}C

Both SiO_2 and oxygen gas targets were utilized in this investigation of the ^{16}O(α, ^{8}Be)^{12}C reaction. A ^{8}Be energy spectrum ($\theta_{lab} = 22.5°$) obtained from a SiO_2 target (145 μg/cm^2) at a bombarding energy of 65 MeV is shown in Fig. 5. The observed energy resolution is 400 keV (FWHM) and transitions can be clearly seen to the ground and first excited states of ^{12}C. Several small peaks due to

^{28}Si or a ^{12}C contaminant in the target appear between the two large peaks. The 4^+, 14.08 MeV level[31] in ^{12}C is only weakly populated at this angle; however, transitions to it were observed consistently with moderate strength (see Fig. 6) at most angles. Both the 0^+, 7.65 MeV level and the 3^-, 9.64 MeV level are not significantly populated at 22.5° although they were regularly observed with weak strength (see Fig. 6). Furthermore, over the angular region investigated, no evidence was discerned for the population of the 2^-, 11.83 MeV or 1^+, 12.71 MeV unnatural parity states; the 1^-, 10.84 MeV level; or the T = 1 states above 15 MeV excitation.

The observed weak population of the 3^-, 9.64 MeV state requires an L = 3 transfer for the simplest case of α-particle pickup. According to equations 1 and 2 such a transfer is impossible if all four particles are transferred within the 1p shell. However, this state may be formed via known 2p-2h and 4p-4h admixtures[33] in the ground state wave function of ^{16}O or via possible[34] 1s shell components in the ^{12}C 3^- state wavefunction. Alternatively, the 3^- state could be excited in a multistep or compound nucleus process so that its relative population may give an indication of the importance of such a process relative to a direct transfer. It should be noted that the ratio of the peak cross section of the 3^- relative to the ground state at this energy is 0.37 whereas at lower bombarding energies[17] this ratio was observed to be ∿1.

Angular distributions of the (α, ^{8}Be) reactions to the ^{12}C(g.s.), 4.44, 7.65, 9.64 and 14.08 MeV states are given in Fig. 6. Both the L = 0 ground state transition and the L = 2 transition to the 4.44 MeV level show oscillatory behavior. The angular distributions for the three higher excited states are fairly structureless with the cross sections increasing slightly at forward angles.

B. $^{15}N(\alpha, ^{8}Be)^{11}B$

At an incident energy of 72.5 MeV, the $^{15}N(\alpha, ^{8}Be)^{11}B$ reaction was studied with a simple identifier[19] which did not require a subnanosecond coincidence between the two ΔE detectors. In Fig. 7a is shown a typical spectrum obtained at a gas pressure of 0.27 atm. Because the effective area of the PSD used in this experiment was only 10×10 mm^2, it was necessary to place the counter telescope close to the gas cell wall to obtain a reasonable detection efficiency (see Table I). The resulting extended target, along with straggling in the cell windows, caused the poor energy resolution of $\sim$800 keV. The $3/2^-$, ground; $1/2^-$, 2.12 MeV; $5/2^-$, 4.44 MeV and $7/2^-$, 6.74 MeV states[31] have large theoretical S_α (see Table III) and strong transitions are seen at these excitation energies in Fig. 7a. Although the $5/2^-$, 4.44 MeV and $3/2^-$, 5.02 MeV levels are not resolved in this spectrum, they were resolved at $\theta_{lab} = 15^\circ$ showing population of the former. In addition, the measured excitation energy of $4.50 \pm .07$ MeV for this combined peak indicates that the $5/2^-$ state (which has the larger theoretical S_α) was systematically populated more strongly than the $3/2^-$ state.

No evidence was observed for transitions to the two positive parity states at 7.29 and 7.98 MeV. Thus a third positive parity level at 6.79 MeV was assumed not to be populated, and transitions to the peak observed at 6.75 MeV are attributed to the expected strong transition to the known $7/2^-$ level at 6.74 MeV.

Angular distributions corresponding to transitions to the first four peaks of Fig. 7a are discussed in Section IV. Since the ^{15}N ground state has a J^π of $1/2^-$, transitions to all final states in ^{11}B should correspond to unique L values; however, no strong oscillatory behavior was observed.

C. $^{14}N(\alpha, ^{8}Be)^{10}B$

A brief survey of the $(\alpha, ^{8}Be)$ reaction on a $^{14}N_2$ gas target was carried out at an incident energy of 72.5 MeV with the same identifier[19] as for ^{15}N. Three angles were studied between $\theta_{lab} = 18° - 28°$ with an energy resolution of $\sim$800 keV. An energy spectrum taken at $\theta_{lab} = 18°$ is shown in Fig. 7b; the predicted locations of transitions to states below $\sim$6 MeV excitation are indicated. No evidence was observed for the excitation of the T = 1 states[32] occuring at 1.74 and 5.17 MeV in accordance with the $\Delta T = 0$ selection rule. Strong transitions were observed to the 3^+, ground; 1^+, 2.15 MeV; and 2^+, 3.59 MeV states, all of which have reasonably large theoretical S_α (see Table III). The observed state at 6.07 ± .08 MeV may correspond to the known 4^+ level at 6.02 MeV which has a large theoretical S_α. A weak transition was observed to the 1^+, 0.72 MeV state and a very weak one to the 3^+, 4.77 MeV state; no transitions above background were observed to the 1^+, 5.18 MeV state, which has a small theoretical S_α.

The available angular distribution data span a very limited angular range and are discussed in Section IV. Over this restricted region the magnitudes of the experimental angular distributions for the four strongly populated states are similar.

D. $^{13}C(\alpha, ^{8}Be)^{9}Be$

A representative spectrum of the $^{13}C(\alpha, ^{8}Be)^{9}Be$ reaction induced by 65 MeV α-particles and with a energy resolution of 480 keV is shown in Fig. 8a. A 135 $\mu g/cm^2$ self-supporting ^{13}C target was used. There are four states in ^{9}Be below 7 MeV excitation which have large theoretical S_α. Strong transitions to two of these levels (the $3/2^-$, ground state and the $5/2^-$, second excited state[32]) dominate the experimental spectrum. As expected for the pickup of an α-cluster in the 1p shell, the $1/2^+$, 1.68 MeV state is not populated nor is the $(3/2)^+$ level

at 4.70 MeV. If the additional positive parity $5/2^+$, 3.06 MeV level was also not populated, transitions to the broad $1/2^-$, 2.78 MeV state account for the small shoulder on the $5/2^-$, 2.43 MeV peak. Transitions to the broad (Γ = 2.0 MeV) $7/2^-$, 6.76 MeV peak could not be observed above background. Since the ^{13}C ground state has a $J^\pi = 1/2^-$, transitions to all final states in ^9Be correspond to unique L values. Angular distributions for the L = 2 transitions to the $3/2^-$ and $5/2^-$ levels are given in Section IV; quite flat distributions were observed.

E. $^{12}C(\alpha, ^8Be)^8Be$

A ^8Be energy spectrum of the $^{12}C(\alpha, ^8Be)^8Be$ reaction taken at $\theta_{lab} = 25°$ is shown in Fig. 8b. This spectrum was obtained by bombarding a 200 $\mu g/cm^2$ carbon target with 65 MeV α particles. The observed energy resolution of the ^8Be ground state peak in Fig. 8b is 450 keV. Transitions can clearly be seen to the 0^+, ground and 2^+, first excited states[32] with possible evidence for weak population of the broad ($\Gamma \sim 3.5$ MeV) 4^+ level at 11.4 MeV. At E_α = 72.5 MeV stronger evidence was observed for the population of this 4^+ level. However, the 2^+ (mixed isospin) states at 16.63 and 16.91 MeV were not observably populated; Marion and Wilson[35] have shown that these states have a dominant single particle nature. An upper limit of 10% of the ground state strength could be placed on the population of these mixed isospin levels which is consistent with their small theoretical S_α relative to that of the ground state (see Table III).

Experimental angular distributions of the transitions to the ground and first excited states of ^8Be are discussed in Section IV. The L = 0 and L = 2 transfer both show oscillatory behavior.

F. $^{11}B(\alpha, ^{8}Be)^{7}Li$

The $^{11}B(\alpha, ^{8}Be)^{7}Li$ reaction was investigated briefly at E_α = 72.5 MeV ($\theta_{lab} = 20°$) and more completely at E_α = 65 MeV. Target thicknesses are given in Table II. Results at both energies are very similar and the ^{8}Be energy spectrum obtained at the higher energy is shown in Fig. 9a. Strong transitions to the $3/2^-$, ground and $7/2^-$, 4.63 MeV states[32] are observed and weak ones to the $1/2^-$, 0.48 MeV state and the two $5/2^-$ states at 6.68 and 7.47 MeV. The ground and first excited states are poorly resolved and there is a sizable uncertainty (20%) in the strength of the transition to the latter although it is populated with surprising strength (see Table III). States above 8 MeV excitation are very weakly populated and an upper limit of ∿6% of the ground state strength can be determined for these states. This limit is consistent with the small calculated S_α for the $3/2^-$, 10.25 MeV state and the $\Delta T = 0$ selection rule which forbids populating the $3/2^-$, T = 3/2, 11.25 MeV state.

At 65 MeV, angular distributions were obtained for the strong transitions populating the $3/2^-$, ground and $7/2^-$, 4.63 MeV states of ^{7}Li. These transitions involve two L transfers and the angular distributions (see Section IV) are rather structureless with an almost constant amplitude.

G. $^{10}B(\alpha, ^{8}Be)^{6}Li$

An investigation of this reaction was carried out by bombarding a 150 $\mu g/cm^2$ self-supporting ^{10}B(98%) target with 72.5 MeV α particles. As seen in Fig. 9b only two ^{6}Li levels,[32] the 1^+, ground state and the 3^+, 2.18 MeV level are observed. This spectrum is dominated by transitions to the 3^+ level which has a large theoretical S_α (see Table III). Predicted locations for transitions to the 2^+, 4.31 MeV and 1^+, 5.7 MeV states and the T = 1 states at 3.56 MeV and 5.37 MeV are also indicated. An upper limit of 4% of the strength to the first excited state can be set on the population of these levels.

Kurath[9] predicts small S_α for the former two states, while Rotter's[8] predicted large S_α are inconsistent with the experimental evidence (see Table III). Transitions to the T = 1 states are forbidden by the $\Delta T = 0$ selection rule. It should be noted that the ^{6}Li(g.s.) is populated fairly weakly in accordance with its small S_α (see Table III). The angular distributions of the transitions to both the ground and first excited states of ^{6}Li have an almost constant amplitude (see Section IV). Due to the 3^+ spin of the ^{10}B (g.s.), multiple L values are allowed in both of these transitions.

H. ^{9}Be(α, ^{8}Be)^{5}He

The ^{9}Be(α, ^{8}Be)^{5}He reaction was observed at several forward angles at a bombarding energy of 65 MeV. In Fig. 10 is shown a ^{8}Be energy spectrum which was obtained at $\theta_{lab} = 24^\circ$ by irradiating an 130 $\mu g/cm^2$ ^{9}Be target. Only the $3/2^-$, ground state[32] of ^{5}He, which has a large theoretical S_α, was observed (see Table III). The $1/2^-$, 4 MeV level, which has a small S_α, is difficult to observe because of the large background and its broad width (Γ = 4 MeV). The narrow $3/2^+$, 16.76 MeV level is not a simple 1p shell state and, as expected, is not observably populated.

I. Excitation Functions

A direct reaction mechanism should give rise to a smooth variation of the shape and magnitude of the differential cross section with increasing bombarding energy. To determine in particular the nature of the ^{12}C(α, ^{8}Be)^{8}Be g.s. reaction near 65 MeV, an excitation function was studied and measurements in small angular steps were taken over the maximum in the angular distribution near $\theta_{c.m.} = 35^\circ$. Data obtained at E_α = 63.2, 65.2, 65.8, 66.6 and 67.3 MeV are shown in Fig. 11a. The angular width of each data point is $\sim 1^\circ$ and the error bars shown are statistical. Upon examining Fig. 11a, it is clear that the magnitude

of the differential cross section is a smooth and slowly decreasing function of the bombarding energy. The shape of the two observed maxima varies slowly with the incident energy.

An excitation function of the (α,^{8}Be) reaction on ^{16}O was also established. Transitions to the ground state of ^{12}C were measured at incident α energies of 55, 60, 65, and 72.5 MeV. The behavior of the data taken at E_α = 65 and 72.5 MeV, the latter over a limited angular region, is similar to that observed on ^{12}C. However, the angular distribution at 55 MeV is quite different from that at the higher two energies and 60 MeV may be a transition region. Thus, at E_α = 55 MeV, processes other than direct ones could be important in the ^{16}O(α,^{8}Be)^{12}C g.s. reaction; this was the conclusion reached by Brown et al.[17] for incident energies over the range 35 - 42 MeV. It is possible, of course, that this difference partly reflects a strong dependence of the direct transfer amplitude on the entrance channel optical potential and on the momentum distribution[36] of the bound α particle in ^{16}O. However, it would appear from the overall spectroscopic selectivity that we observe and the behavior of the angular distributions at 65 MeV and above that the reaction is predominantly direct in this energy region.

J. Comparison of (α,^{8}Be), (d,^{6}Li), (^{3}He,^{7}Be) and (α,2α) Reactions

The relative population of final states by the (α,^{8}Be) reaction on 1p shell nuclei is in general in good agreement with the previously reported (d,^{6}Li) and (^{3}He,^{7}Be) results at high bombarding energies[15,37] and with the assumption that these reactions proceed via a direct α-cluster transfer. Only final states with the same parity as the target were appreciably populated with the notable exception of the 3^-, 9.64 MeV level in ^{12}C, which was made with moderate strength by all three reactions. In general the three pickup reactions

strongly populated only final states with significant theoretical S_α. Transitions to the mixed isospin 2^+ levels at 16.63 and 16.91 MeV in ^{8}Be comprise an exception to this rule. These levels were not seen in the (α, ^{8}Be) reaction, as expected from their very small α-particle spectroscopic factors, whereas both the (d, ^{6}Li) and (^{3}He, ^{7}Be) reactions populated them with moderate strength. From a comparison of the 1p shell systematics for these α-pickup reactions, it seems clear that a direct mechanism dominates at high energies. However, the (α, ^{8}Be) reaction appears to be somewhat more selective in populating predominantly final states with the same parity as the target and in only populating levels with large α-particle spectroscopic factors.

Since the (α, ^{8}Be) and the (α,2α) reactions share the same entrance channel and have very similar exit channels, it is interesting to compare these reactions on ^{12}C and ^{16}O targets. A very prominent systematic feature observed in a study of the (α,2α) reaction on even-even 1p shell and 2s1d shell targets at E_α = 90 MeV[16] was the predominance of the ground state transition at the symmetric quasi-elastic angle. In fact the ^{8}Be and ^{12}C ground states were observed in the (α,2α) data to be populated a factor of two and four, respectively, larger than their first excited states. In contrast, the (d, ^{6}Li), (^{3}He, ^{7}Be) and (α, ^{8}Be) reactions all preferentially populated the ^{8}Be (2.94 MeV) state larger than its ground state and populated the ^{12}C (4.44 MeV) state a factor of 3 to 4 times stronger than its ground state. This apparent disagreement has been resolved by Chant and Roos[38] who showed that the low excited state cross sections were the result of distortion effects.

IV. ANALYSIS AND DISCUSSION

The selectivity of final states populated by the $(\alpha, {}^{8}Be)$ reaction and, the smooth dependence of the shape of its differential cross section on the bombarding energy (at or above 65 MeV) imply that this reaction can be analyzed in the framework of direct reaction theory, i.e., via the distorted-wave Born-approximation (DWBA). The application of this theory is based on the assumption that the reaction proceeds by a one step pickup of an "α-cluster" (2 correlated protons and neutrons in an S = T = 0 state).

A. DWBA Calculations

In the distorted-wave Born approximation, the differential cross section for the reaction $B(\alpha, {}^{8}Be)A$ is given by:

$$\frac{d\sigma}{d\Omega}(\Theta) = \sum_{L} S^{L}(B \rightarrow A+\alpha)\ S({}^{8}Be \rightarrow \alpha+\alpha)\ \sigma^{L}_{DWBA}(\Theta) \qquad (3)$$

where L runs over all the allowed angular momentum transfers according to Equation 2. The kinematic part of the cross section, σ^{L}_{DWBA}, was calculated using DeVries' EFR-DWBA code LOLA.[39] The optical model potentials needed to generate the distorted waves in the entrance and exit channels were determined by fitting tabulated α-particle elastic scattering data on ^{12}C, ^{13}C, ^{14}N and ^{15}N at 40.5 MeV[40] and on ^{16}O at 65 MeV[41] with the search code GENOA[42]. The scattering data for each target were fit individually with Woods-Saxon potentials having both real and imaginary volume terms. For each of the targets ^{13}C, ^{14}N and ^{15}N there was a single potential, given in Table IV, which gave the lowest chi-squared fit to the scattering data on that target. For ^{12}C and ^{16}O, two or more potentials fit the elastic data equally well and thus the one which best reproduced the shape of the $(\alpha, {}^{8}Be)$ angular distributions was selected (see Table IV). The sensitivity of the shape of the calculated cross sections

to the entrance channel potential made this choice straightforward. For the ^{9}Be, ^{10}B and ^{11}B targets no tabulated scattering data were available in the appropriate energy region. Thus a potential from the literature[43] (similar to the above ^{13}C one, see Table IV) which reproduced 46 MeV α-scattering on ^{11}B was used.

In order to approximate a potential for the particle-unstable ^{8}Be, GENOA was used to determine an optical potential which reproduced 50 MeV ^{9}Be elastic scattering data[44] on ^{12}C (potential AA in Table IV). A second potential with a larger real well depth was also tried. This latter potential caused a small change in the magnitude of the fits and virtually no change in the shape. Since the $^{16}O(\alpha, ^{8}Be)^{12}C$ reaction calculations were found to be relatively insensitive to the exit channel potential and no ^{9}Be elastic scattering data existed for the other exit channels, potential AA was used to generate the distorted waves in the ^{8}Be channel for all of the lp shell targets.

The bound state wave functions which describe the motion of an α cluster in the target nucleus B and in ^{8}Be were calculated in the usual way using a real Woods-Saxon potential whose well depth was adjusted to give the observed α binding energy. The radius of the Woods-Saxon well describing the target nuclei was chosen to be $R = r_o A^{1/3}$. An r_o of 2.0 was used for all targets; this gave a radius which was larger than the physical size of the core A. This larger radius could correspond to the transferred α-particle existing at the surface of the core. Decreasing r_o from 2.0 to 1.2 had only a small effect on the shape of the fits but caused a strong decrease in the magnitude of the cross section.

Although ^{8}Be is unbound by 92 keV, it is effectively bound by its Coulomb barrier during the reaction time. To generate a bound state wave function for the calculations, it was assumed that the ^{8}Be internal wave function varied smoothly and slowly when its binding energy was changed from -92 keV to +10 keV.

The ^{8}Be internal wave function was then calculated for an α particle bound to a second one by 10 keV in a Woods-Saxon well with a radius of 3.2 fm. (Changing the binding energy from 100 keV to 10 keV produced no change in the shape of the calculated cross sections and only a 7% decrease in their magnitudes.)

In deriving experimental spectroscopic factors, we have tried to maintain consistent criteria for choosing the center of mass angle at which to relate experiment and theory, since the shapes of the calculated and experimental cross sections are not identical. If an experimental maximum existed in the angular distribution, the theoretical and experimental yields were compared at this angle. For the flatter angular distributions, the spectroscopic factor was calculated at a data point between $\theta_{c.m.}$ = 25 and 35°. A comparison of the experimental S_α with Kurath's theoretical ones[9] is presented in Table V.

The values of the theoretical α-particle spectroscopic factors $S^{L}(B\rightarrow A+\alpha)$ in Eq. 3 were taken from Kurath[9] and from Rotter[8]. For $S(^{8}Be\rightarrow\alpha+\alpha)$ the theoretical value of 1.5 was taken from Kurath[9]. The calculated cross sections and the experimental data are shown in Figs. 12 to 17 and are discussed in the following section.

B. Comparison of Theoretical and Experimental Cross Sections

For most nuclei, Kurath's[9] and Rotter's[8] spectroscopic factors are in good agreement. Since Kurath gives spectroscopic factors for all the 1p shell targets, the theoretical cross sections shown were calculated using his values unless otherwise noted. For Figs. 12-17 the width of each data point corresponds to the angular acceptance of the ^{8}Be identifier used in the measurement. Furthermore, if the statistical error exceeded the height of the data point, it is given in the figure.

1. $^{16}O(\alpha, ^{8}Be)^{12}C$

A comparison of the $(\alpha, ^{8}Be)$ experimental (symbols) and absolute calculated (solid curves) cross sections for transitions populating the ^{12}C ground state and several excited states is shown in Fig. 12. The similar magnitudes of the experimental and calculated cross sections demonstrate good agreement between the theoretical α-particle spectroscopic factors and experiment (see Table V). The shapes of the theoretical cross sections reproduce some of the features of the experimental data - most notably the relative spacing and magnitude of the two forward maxima in the ground state angular distribution. Furthermore, the damping of the oscillatory character observed experimentally in the L = 2 and L = 4 angular distributions, compared to that of the L = 0 ground state, is also reproduced by the calculations.

2. $^{15,14}N(\alpha, ^{8}Be)^{11,10}B$

For the ^{15}N target the magnitudes of the experimental and theoretical cross sections are generally in fair agreement (see Fig. 13). The structureless shapes of the experimental L = 2 and 4 angular distributions are qualitatively reproduced by the calculations, but the theoretical L = 0 angular distribution shows more pronounced oscillations than does experiment.

Over the very limited angular range studied on the ^{14}N target, the experimental cross sections are structureless and relatively constant (see Fig. 14). The theoretical calculations generally reproduce this feature as well as the cross section magnitudes. It should be noted that all of these transitions to ^{10}B have an angular momentum transfer of 2 or greater. For transitions involving more than one L value, the incoherent sum of the contributions to the cross section from both values is shown in Fig. 14.

3. $^{13,12}C(\alpha,^{8}Be)^{9,8}Be$

The structureless shapes of the ^{13}C data (see Fig. 15) are reproduced by the calculated cross sections although the yields are overestimated at forward angles and underestimated at backward ones. The shapes of the angular distributions observed from the ^{12}C target (see Fig. 15) are poorly reproduced by the fits which severely overestimate the magnitude of the cross section at forward angles. However, the magnitudes do agree in the region of the experimentally observed maxima near 40°.

4. $^{11,10}B(\alpha,^{8}Be)^{7,6}Li$ and $^{9}Be(\alpha,^{8}Be)^{5}He$

For the ^{11}B, ^{10}B and ^{9}Be targets, two or more values of L are allowed. Fig. 16 shows two examples which illustrate the relative contributions from each L value to the shape and magnitude of the theoretical cross section (Rotter's[8] values of S^L were used). The transition to the ^{6}Li ground state can proceed by the pickup of an α particle with an angular momentum of 2 or 4 with the L = 4 component making the dominant contribution; for the ^{7}Li(g.s.), L = 0 or 2, with the L = 2 component dominant. Since the kinematic factors for L = 0, 2 or 4 transfer are comparable, the magnitude of the cross section for a particular L value in these two cases directly reflects the magnitude of the theoretical S_α.

For reactions on ^{10}B the theoretical S_α of Kurath and of Rotter differ somewhat, though for reactions on ^{9}Be and ^{11}B they are very similiar (see Table III). In Fig. 17, calculated curves using both Kurath's[9] (solid) and Rotter's[8] (dashed) S_α are presented. Disagreement with experiment is greatest for the transition to the ^{6}Li (g.s.); however, the difference is small in absolute magnitude since the transition is predicted to be very weak. The magnitudes of the calculated cross sections are roughly comparable to the experimental ones for the transitions

to the ^{6}Li (2.18 MeV), ^{7}Li (g.s.) and ^{7}Li (4.63 MeV states; however, the flatness of the experimental data is not reproduced. For the very limited ^{9}Be target data the theoretical curve follows the slope but overestimates the magnitude of the differential cross sections. The poorer quality[45] fits for the reactions on the ^{9}Be, ^{10}B and ^{11}B targets could be due in part to the fact that the exit channel elastic scattering may not be well described by potential AA (see Table IV), which was obtained from ^{9}Be scattering on ^{12}C. In addition the reaction calculations are sensitive to the entrance channel optical parameters, but α-particle scattering data on ^{9}Be and ^{10}B were not available and thus potential E (derived from α-scattering on ^{11}B) was used of necessity.

C. General Comparison of Theoretical and Experimental α-Particle Spectroscopic Factors

In Fig. 18a are shown ratios R^{abs} of experimental to theoretical S_α (see also Table V) where R^{abs} is defined by:

$$R^{abs} = \frac{S(exp)}{S(theory)} = \frac{d\sigma/d\Omega\ (\Theta)_{exp}}{d\sigma/d\Omega\ (\Theta)_{th}} .$$

For consistency, Kurath's theoretical α-particle spectroscopic factors[9] are used for all targets. In general these ratios lie below the dashed line at $R^{abs} = 1.0$, but deviate from it by less than 50%. (Of course this comparison is very sensitive to systematic errors either in the experimental data or in the reaction calculations; an example of the latter is that the magnitude of the calculated cross section is affected by the value of r_o used in calculating the bound state wave functions). The ^{6}Li (g.s.) point is off-scale because of its very small theoretical S_α.

In order to minimize systematic errors, the above ratio of spectroscopic factors, R^{abs}, was divided by the ratio for the ground state transition. The ratio R^{rel} is defined by:

$$R^{rel} = \frac{R^{abs}(B \rightarrow A + \alpha)}{R^{abs}(B \rightarrow A\ (g.s.) + \alpha)} \quad . \tag{5}$$

Part b of Fig. 18 presents this relative ratio of S_α; R^{rel} is again plotted against the final state populated. Better agreement between experiment and theory is seen in Fig. 18b in that the values of R^{rel} cluster closer to 1 than those for R^{abs} in Fig. 18a with only four values of R^{rel} farther than ± 50% from unity, the ^{6}Li(g.s) point is again off scale. Relative spectroscopic factors for the individual transitions are also presented in Table VI.

Several previous investigators have measured α-particle spectroscopic factors for the ground state to ground state transitions utilizing the (d,^{6}Li), (^{3}He,^{7}Be) and (α,2α) reactions on 1p shell targets. These results were typically reported as relative spectroscopic factors normalized to 1 for the $^{12}C \rightarrow {}^{8}Be$ (g.s.) transition. In Table VII[46-48] two theoretical and several experimental S_α are compared (with $S(^{12}C \rightarrow {}^{8}Be\ (g.s.) + \alpha) = 1$) ; it can be seen that the two theoretical predictions are very similar.

Comparing the experimental spectroscopic factors to the theoretical ones, it is clear that the (α,^{8}Be) results are in moderate agreement with theory, particularly on the heavier targets. Some scatter is observable in the various (d,^{6}Li), (^{3}He,^{7}Be) and (α,2α) data in the table. However, the agreement among some of the experimental measurements is encouraging considering the different reactions and the wide range of bombarding energies employed. The experimentally observed strength to the ^{6}Li (g.s.) may indicate that ^{10}B has a larger amount of this parentage than is theoretically predicted; however, since this transition is predicted to be very weak, other reaction mechanisms which are normally negligible could account for some of the observed strength.

V. SUMMARY AND CONCLUSIONS

An investigation of the (α,^{8}Be) reaction at high bombarding energies on all stable 1p shell target nuclei has been presented. This study has shown that the (α,^{8}Be) reaction can be understood in terms of a simple α-cluster pickup process which has been previously used to describe successfully the major features of the (d,^{6}Li) and (^{3}He,^{7}Be) reactions. A systematic feature which emerged from this investigation was the strong population of only those states which are predicted to have significant α-particle spectroscopic factors. This selectivity is evidence that the (α,^{8}Be) reaction proceeds via a simple α-cluster pickup process. The relative population of final states via the (α,^{8}Be) reaction on 1p shell nuclei was generally in good agreement with the previously reported (d,^{6}Li) and (^{3}He,^{7}Be) results. However, a notable exception to this arose in that, while no population of the mixed isospin states at $\sim$16 MeV in ^{8}Be by the ^{12}C(α,^{8}Be) reaction was expected or observed, both the (d,^{6}Li) and (^{3}He,^{7}Be) reactions moderately populate these levels of dominant single-particle character.

The probable occurence of a cluster pickup mechanism for the (α,^{8}Be) reaction greatly simplifies the theoretical description. In order to extract α-particle spectroscopic factors for comparison with theory, the data were analyzed with exact-finite range DWBA. These reaction calculations were found to be sensitive to the optical potential describing the entrance channel elastic scattering, but rather insensitive to the exit channel potential. Both absolute and relative spectroscopic factors were extracted for 22 states which are generally in good agreement with the theoretical predictions of both Kurath[9] and Rotter[8] as to the extent of α-clustering in these light nuclei.

The selectivity and good quantitative agreement with theoretical predictions illustrate that the (α, ^{8}Be) reaction is a useful spectroscopic probe with which to measure the extent of α-clustering in nuclei. Furthermore the large solid angle ^{8}Be identifier described within will facilitate similiar studies on heavier nuclei.

ACKNOWLEDGMENTS

We wish to thank D. Landis for designing the fast/slow preamplifiers, J. Walton for fabricating the transmission detectors, Dr. M. Nagarajan for many informative discussions on direct reaction theory and for his keen interest throughout the duration of this work, and Dr. George Delic for checking some of our EFR-DWBA calculations with his reaction code KUNDRY and for several helpful discussions on optical model potentials.

FOOTNOTES AND REFERENCES

*Work performed under the auspices of the U. S. Energy Research and Development Administration.

1. E. P. Wigner, Phys. Rev. 51, 106 (1937).
2. D. H. Wilkinson, Proc. Rutherford Jubilee Int. Conf., Manchester, ed. J. Birks (Heywood & Co. LTD. 1961) p. 339
3. G. A. Wheeler, Phys. Rev. 52, 1083 (1937).
4. K. Wildermuth and W. McClure, in Springer Tracts in Modern Physics, Vol. 41 (Springer-Verlag, Berlin, Heidelberg, New York, 1966).
5. D. M. Brink , Proc. of International School of Physics, 'Enrico Fermi' 1965 (C. Block, ed.) Academic Press, New York and London (1966), p247.
6. A. Arima, H. Horiuchi, K. Kubodera and N. Takigawa, Advances in Nuclear Physics, Vol. 5 (M. Baranger and E. Vogt, eds) Plenum Press, New York 1973), 345.
7. D. M. Brink, Proceedings of the Second Inter. Conf. on Clustering Phenomena in Nuclei, (ed. by D. A. Goldberg, J. B. Marion and S. J. Wallace), National Information Service, U. S. Dept. of Commerce, Springfield, Virginia, (1975) p. 3. Also, see other references in these proceedings.
8. I. Rotter, Fortschr. Phys. 16, 195 (1968).
9. D. Kurath, Phys. Rev. C7, 1390 (1973).
10. K. Bethge, Ann. Rev. of Nucl. Sci. 20, (1970).
11. J. D. Garrett in the Proceedings of the Symposium on Two-Nucleon Transfer and Pairing Excitations, Argonne Physics Division Informal Report PHY- 1972H 232 (1972).
12. F. D. Becchetti, L. T. Chua, J. Jänecke and A. M. Vandermolen, Phys. Rev. Lett. 34, 225 (1975).
13. H. H. Gutbrod, H. Yoshida and R. Bock, Nucl. Phys. A165, 240 (1971).
14. G. Audi, C. Détraz, M. Langevin and F. Pougheon, Nucl. Phys. A237, 300 (1975).
15. W. F. Steele, P. A. Smith, J. E. Finck and G. M. Crawley, preprint (MSUCL-186).
16. J. D. Sherman, D. L. Hendrie, and M. S. Zisman, Phys. Rev. C13, 20 (1976).
17. R. E. Brown, J. S. Blair, D. Bodansky, N. Cue, and C. D. Kavaloski, Phys. Rev. 138, B1394 (1965).

18. G. J. Wozniak, N. A. Jelley and Joseph Cerny, Phys. Rev. Lett. 31, 607 (1973).

19. G. J. Wozniak, N. A. Jelley and Joseph Cerny, Nucl. Instr. and Meth. 120, 29 (1974).

20. F. Brochard, P. Chevallier, D. Disdier, V. Rauch, G. Rudolf and F. Scheibling, Phys. Rev. C13, 967 (1976).

21. K. S. Jayaraman and H. D. Holmgren, Phys. Rev. 172, 1015 (1968).

22. G. J. Wozniak, H. L. Harney, K. H. Wilcox and Joseph Cerny, Phys. Rev. Lett. 28, 1278 (1972).

23. J. G. Cramer, K. A. Eberhard, N. R. Fletcher, E. Mathiak, H. H. Rossner and A. Weidinger, Nucl. Instr. and Meth. 111, 425 (1973).

24. J. L. Artz, M. B. Greenfield and N. R. Fletcher, Phys. Rev. C13, 156 (1976).

25. H. Ho, W. Dunnweber, D. Dehnhard, K. Mudersbach and J. P. Wurm, Nucl. Phys. A233, 361 (1974).

26. A. Menchaca-Rocha, Nucl. Instr. and Meth. 114, 425 (1974).

27. Tests with an α-particle source demonstrated that no false coincidences were generated by particles passing through the 1 mm dead region between the twin ΔE detectors and thus collimation of this region was unnecessary.

28. Due to the very low background attainable with the ΔTOF and PI requirements, a comparison of the energy losses in the twin ΔE detectors was not used; this approach is discussed in Ref. 19.

29. Our PSDs were obtained from Edax International, Inc.

30. Copies of this program are available from the authors upon request.

31. Quoted excitation energies, spin and parity assignments for states in ^{12}C and ^{11}B are taken from F. Ajzenberg-Selove, Nucl. Phys. A248, 1 (1975).

32. Quoted excitation energies, spin and parity assignments for states in ^{10}B, ^{9}Be, ^{8}Be, ^{7}Li, ^{6}Li and ^{5}He are taken from F. Ajzenberg-Selove and T. Lauritsen, Nucl. Phys. A227, 1 (1974).

33. J. Lowe, A. R. Polletti and D. H. Wilkinson, Phys. Rev. 148, 1045 (1966).

34. A. A. Pilt, private communication.

35. J. B. Marion and M. Wilson, Nucl. Phys. 77, 129 (1966).

36. M. A. Nagarajan, Phys. Lett. 52B, 395 (1974).

37. R. L. McGrath, D. L. Hendrie, E. A. McClatchie, B. G. Harvey and Joseph Cerny, Phys. Lett. 34B, 289 (1971).

38. N. S. Chant and P. G. Roos, Proceedings of the Second Inter. Conf. on Clustering Phenomena in Nuclei, ed. by D. A. Goldberg, J. B. Marion and S. J. Wallace, (1975) p. 265.

39. R. M. DeVries, Phys. Rev. C8, 951 (1973).

40. B. G. Harvey, J. R. Meriwether, J. Mahoney, A. Bussiere De Nercy and D. J. Horen, Phys. Rev. 146, 146 (1966). See University of Calif. Radiation Laboratory report # 16573 for tabulated data.

41. B. G. Harvey, E. J-M. Rivet, A. Springer, J. R. Meriwether, W. B. Jones, J. H. Elliott and P. Darriulat, Nucl. Phys. A52, 465 (1964). D. L. Hendrie, private communication.

42. F. G. Perey, optical-model search code (unpublished).

43. B. Zeidman, H. T. Fortune and A. Richter, Phys. Rev. C2, 1612 (1970).

44. G. J. Wozniak, D. P. Stahel, B. Jeltema, M. S. Zisman and Joseph Cerny, to be published.

45. A further complication arises in the $(\alpha, ^{8}Be)$ reaction on ^{9}Be, ^{10}B and ^{11}B targets in that contributions are possible from simple pickup reactions--i.e. $^{10}B(\alpha, ^{6}Li)^{8}Be$--in the backward hemisphere. Unfortunately no data are available for this bombarding energy and angular region from which to estimate their contribution.

46. M. Bedjidian, M. Chevallier, J. Y. Grossiord, A. Guichard, M. Gusakow, J. R. Pizzi and C. Ruhla, Nucl. Phys. A189, 403 (1972).

47. L. J. Denes, W. W. Daehnick and R. M. Drisko, Phys. Rev. 148, 1097 (1966).

48. C. Détraz, H. H. Duhm and H. Hafner, Nucl. Phys. A147, 488 (1970).

Table I. ^{8}Be Identifier geometry for several different experiments.

Experiment	Target to PSD Distance (cm)	Collimator[a]	Diameter[a] (cm)	Width[a] (cm)	Height[a] (cm)	Post or Gap-width[b] (cm)	Position Gate-width[c] (cm)	Acceptance Angle (^{8}Be) (deg)
I	8.00	circular	.83	-	-	.28 (V)	.12	0.9
II	13.00	rectangular	-	1.12	1.25	.30 (V)	.25	1.1
III	7.45	gas[d]	-	.78	.81	.24 (V)	.26	2.0
IV	13.35	rectangular	-	1.51	.98	.19 (V)	.53	2.3
V	13.05	rectangular	-	2.00	.99	.09 (H)	1.07	4.7

[a] Projected dimensions of the collimator on the PSD.

[b] Projected dimension on the PSD of the divided collimator[19] post-width or the gap-width of the undepleted region[19] between the twin transmission detectors. The letters V or H indicate whether the gap was vertical (V) or horizontal (H).

[c] If more than one position gate was set, only the summed width is given.

[d] The distances from the target to the gas collimator (L_1) and from this collimator to the second one (L_2) were 3.60 cm and 3.85 cm, respectively. Only the dimensions of the second collimator are listed above. The dimensions of the width, height and post of the front gas collimator were 0.38 cm, 0.38 cm and 0.12 cm, respectively.

Table II. Solid and gas target thicknesses.

Experiment	E_α (MeV)	Solid Targets ($\mu g/cm^2$)						Gas Targets Pressure (atm)		Gas Targets Temperature (^0C)	
		^9Be	^{10}B	^{11}B	^{12}C	^{13}C (90%)	^{16}O[a]	$^{14}N_2$	$^{15}N_2$	$^{14}N_2$	$^{15}N_2$
I	65.0			100	50		220				
II	72.5		150	100	305		210				
III	72.5				305			.33	.27	27	27
IV	65.0	130			200	135	145				
V	60.0						240				

[a] Thickness of SiO_2 targets.

Table III. Experimental peak (α, ^{8}Be) cross sections for the population of a final state and the predicted α-particle spectroscopic factor for transitions to that state.

Product Nucleus	Known Levels[a]			Observed Levels		Peak Cross Section	S_α	
	MeV	J^π	T	MeV	±keV	μb/sr	Kurath[b]	Rotter[c]
^{12}C	0	0^+	0	0		23	.23	.23
	4.44	2^+	0	4.42	40	42	1.30	1.26
	7.65	0^+	0	7.67	50	3.4	.06	
	9.64	3^-	0	9.65	50	8.6		
	10.3	(0^+)	0			<1		
	10.84	1^-	0			<1		
	11.83	2^-	0			<1		
	12.71	1^+	0			<1		
	13.35	(2^-)	0			<1		
	14.08	4^+	0	14.06	100	13	2.38	2.44
^{11}B	0	$3/2^-$	1/2	0		8.7	.41	
	2.12	$1/2^-$	1/2	2.10	40	11	.20	
	4.44	$5/2^-$	1/2	4.50	70	9.2	.29	
	5.02	$3/2^-$	1/2				.11	
	6.74	$7/2^-$	1/2	6.75	40	9.2	1.09	
	6.79	$1/2^+$	1/2					
	7.29	$(3/2,5/2)^+$	1/2					
	7.98	$3/2^+$	1/2					
^{10}B	0	3^+	0	0		8.6	.70	
	0.72	1^+	0			1.1	.13	
	1.74	0^+	1					
	2.15	1^+	0	2.11	50	5.9	.18	
	3.59	2^+	0	3.58	60	6.2	.35	
	4.77	3^+	0	4.76	70	1.0	.05	
	5.11	2^-	0					

(continued)

Table III. (continued)

Product Nucleus	Known Levels[a]			Observed Levels		Peak Cross Section	S_α	
	MeV	J^π	T	MeV	±keV	μb/sr	Kurath[b]	Rotter[c]
^{10}B	5.17	2^+	1					
	5.18	1^+	0				.07	
	5.92	2^+	0					
	6.02	4^+		6.07	80	7.2	.40	
	6.13	3^-						
^{9}Be	0	$3/2^-$	1/2	0		19.4	.41	
	1.68	$1/2^+$	1/2					
	2.43	$5/2^-$	1/2	2.39	40	9.2	.22	
	2.78	$1/2^-$	1/2			4	.22	
	3.06	$5/2^+$	1/2					
	4.70	$(3/2)^+$	1/2					
	6.76	$7/2^-$	1/2				.23	
^{8}Be	0	0^+	0	0		50	.56	.54
	2.94	2^+	0	2.96	70	75	.71	.68
	11.4	4^+	0				.77	.68
	16.63	2^+	0+1			<6	.06	
	16.91	2^+	0+1					
^{7}Li	0	$3/2^-$	1/2	0		18.3	.65	.55
	0.48	$1/2^-$	1/2	.52	50	4.0	.002	
	4.63	$7/2^-$	1/2	4.64	30	7.8	.49	.44
	6.68	$5/2^-$	1/2			3.0	.08	
	7.47	$5/2^-$	1/2	7.46	70	2.6	.07	.06
	9.61	$7/2^-$	1/2			<1		
	10.25	$3/2^-$	1/2			<1	.005	
	11.25	$3/2^-$	3/2			<1		

(continued)

Table III (continued)

Product Nucleus	Known Levels[a]			Observed Levels		Peak Cross Section	S_α	
	MeV	J^π	T	MeV	±keV	μb/sr	Kurath[b]	Rotter[c]
^{6}Li	0	1^+	0	0		6.2	.003	.013
	2.18	3^+	0	2.18	30	28.6	1.06	.37
	3.56	0^+	1			<1		
	4.31	2^+	0			<1	.06	.36
	5.37	2^+	1			<1		
	5.7	1^+	0			<1	.01	.37
^{5}He	0	$3/2^-$	1/2	0		87	1.12	1.15
	4	$1/2^-$	1/2				.06	.03
	16.76	$3/2^+$	1/2					

[a] Refs. 31 & 32.

[b] Ref. 9.

[c] Ref. 8.

Table IV. Optical model potentials used in the DWBA calculations

Target	Projectile	$E_{proj.}$ MeV	V MeV	r_R^a fm	a_R fm	W MeV	r_I^a fm	a_I fm	r_C^a fm	Potential
^{16}O	α	65	89.3	1.56	.57	27.7	1.39	.72	1.2	A[b]
^{15}N	α	40.5	279	1.22	.65	17.6	1.55	.65	1.2	B[c]
^{14}N	α	40.5	279	1.22	.65	17.6	1.55	.65	1.2	B[c]
^{13}C	α	40.5	170	1.47	.55	20.8	1.56	.35	1.2	C[c]
^{12}C	α	40.5	36.7	1.80	.41	7.6	1.96	.66	1.2	D[c]
$^{11}B, ^{10}B, ^{9}Be$	α	46	194	1.38	.60	24	1.60	.60	1.2	E[d]
^{12}C	^{9}Be	50	35.2	1.72	.92	12	2.65	.50	1.2	AA[e]

[a] $R = rA_{tgt}^{1/3}$

[b] Derived from tabulated data in Ref. 41.

[c] Derived from tabulated data in Ref. 40.

[d] Potential for ^{11}B taken from Ref. 43.

[e] Derived from tabulated data in Ref. 44.

Table V. Comparison of experimental and theoretical α-particle spectroscopic factors.

Target	Level (MeV)	Theory[a]			Experiment	
		S^0	S^2	S^4	S_{th}	S_{exp}
^{16}O	^{12}C(g.s.)	.23			.23	.25
	4.44		1.30		1.30	1.07
	7.65	.06			.06	.05
	14.08			2.38	2.38	1.40
^{15}N	^{11}B(g.s.)		.41		.41	.23
	2.12	.20			.20	.12
	4.44		.29		.29	.29
	6.74			1.09	1.09	.45
^{14}N	^{10}B(g.s.)		.012	.69	.70	.41
	2.15	.08	.10		.18	.10
	3.59		.35		.35	.14
	4.77		.044	.004	.05	.04
	6.02			.40	.40	.52
^{13}C	^{9}Be(g.s.)		.41		.41	.37
	2.43		.22		.22	.18
^{12}C	^{8}Be(g.s.)	.56			.56	.55
	2.94		.71		.71	.75
^{11}B	^{7}Li(g.s.)	.26	.39		.65	.19
	4.63		.06	.43	.49	.34
^{10}B	^{6}Li(g.s.)		.000	.003	.003	.16
	2.18	.22	.60	.24	1.06	.42
^{9}Be	^{5}He(g.s.)	.56	.56		1.12	.53

[a]Theoretical S_α from Kurath (Ref. 9). See Table III for Rotter's S_α (Ref. 8).

Table VI. Comparison of experimental and theoretical relative α-particle spectroscopic factors.

Target	Level	S_α^{Rel} theory[a]	S_α^{Rel} experiment
^{16}O	^{12}C(g.s.)	1.00	1.00
	4.44	5.54	4.28
	7.65	.26	.20
	14.08	10.15	5.60
^{15}N	^{11}B(g.s.)	1.00	1.00
	2.12	.50	.52
	4.44	.72	1.26
	6.74	2.68	1.96
^{14}N	^{10}B(g.s.)	1.00	1.00
	2.14	.25	.24
	3.59	.50	.34
	4.77	.07	.10
	6.02	.58	1.27
^{13}C	^{9}Be(g.s.)	1.00	1.00
	2.43	.53	.49
^{12}C	^{8}Be(g.s.)	1.00	1.00
	2.94	1.28	1.36
^{11}B	^{7}Li(g.s.)	1.00	1.00
	4.63	.75	1.79
^{10}B	^{6}Li(g.s.)	.003[b]	.38[b]
	2.18	1.00	1.00
^{9}Be	^{5}He(g.s.)	1.00	1.00

[a] Theoretical S_α from Ref. 9.

[b] The ratio of S_α relative to the 2.18 MeV state is given for $^{10}B \rightarrow {}^{6}Li+\alpha$.

Table VII. Comparison of theoretical and experimental ground state α-particle spectroscopic factors normalized to unity for $S_\alpha(^{12}C \rightarrow {}^{8}Be(g.s.)+\alpha)$.

Target	Theoretical		S_α^{Rel} Experimental							
	Kurath[a]	Rotter[b]	This Work[c] (α,^{8}Be)	Gutbrod[d] ←	Bedjidian[e] (d,^{6}Li)	Denes[f] →	Detraz[g] ←	Audi[h] (^{3}He,^{7}Be)	Steele[i] →	Sherman[j] (α,2α)
^{9}Be	2.00	2.12	.96							
^{10}B	.005	.024	.29	.33						
^{11}B	1.17	1.02	.35	1.62						
^{12}C	1.00	1.00	1.00	1.00	1.00	1.00	1.00	1.00	1.00	1.00
^{13}C	.73		.67			2.0			.44	
^{14}N	1.25		.75							
^{15}N	.73		.42							
^{16}O	.41	.42	.44	.44	.32	5.0	3.3	.64[k]	.97	1.21

[a] Theoretical S_α from Ref. 9.

[b] Theoretical S_α from Ref. 8.

[c] This work (α,^{8}Be) at 65-72.5 MeV.

[d] Ref. 13 (d,^{6}Li) at 19.5 MeV.

[e] Ref. 46 (d,^{6}Li) at 28 MeV.

[f] Ref. 47 (d,^{6}Li) at 15 MeV.

[g] Ref. 48 (^{3}He,^{7}Be) at 30 MeV.

[h] Ref. 14 (^{3}He,^{7}Be) at 26 MeV.

[i] Ref. 15 (^{3}He,^{7}Be) at 70 MeV.

[j] Ref. 16 (α,2α) at 90 MeV.

[k] Average of numbers given in Ref. 14.

Fig. 1. A schematic diagram of the ^{8}Be identifier showing the twin transmission detectors, the PSD, the trajectories of the breakup α-particles (solid lines) and the measured direction X of the ^{8}Be event.

Fig. 2. Differential time of flight ΔTOF (a) and particle identification PI (b) spectra obtained with the ^{8}Be identifier.

Fig. 3. The effective solid angles Ω_{eff} of several different ^{8}Be identifiers (I→V) which were used to study solid targets (solid lines) and gas targets (dashed line). See Table I for a description of the geometries of these identifiers.

Fig. 4. An electronic block diagram for the ^{8}Be identifier.

Fig. 5. An energy spectrum from the $^{16}O(\alpha,^{8}Be)^{12}C$ reaction at $\Theta_{lab} = 22.5°$. The locations of possible transitions to all final states in ^{12}C below 14 MeV excitation are indicated.

Fig. 6. Angular distributions for $(\alpha,^{8}Be)$ transitions to the ground and four excited states of ^{12}C at $E_{\alpha} = 65$ MeV.

Fig. 7. ^{8}Be energy spectra from (a) the $^{15}N(\alpha,^{8}Be)^{11}B$ and (b) the $^{14}N(\alpha,^{8}Be)^{10}B$ reactions at a bombarding energy of 72.5 MeV and laboratory angles of 19° and 18°, respectively. The locations of possible transitions to all final states below ∿ 7 MeV are shown.

Fig. 8. ^{8}Be energy spectra from (a) the $^{13}C(\alpha,^{8}Be)^{9}Be$ reaction at $\Theta_{lab} = 32°$ and (b) the $^{12}C(\alpha,^{8}Be)^{8}Be$ reaction at $\Theta_{lab} = 25°$ at a bombarding energy of 65 MeV. The locations of possible transitions to all final states in ^{9}Be below ∿7 MeV and in ^{8}Be below ∿17 MeV are indicated.

Fig. 9. ^{8}Be energy spectra from (a) the $^{11}B(\alpha,^{8}Be)^{7}Li$ reaction at $\Theta_{lab} = 20°$ and (b) the $^{10}B(\alpha,^{8}Be)^{6}Li$ reaction at $\Theta_{lab} = 24°$, both employed a bombarding energy of 72.5 MeV. The locations of possible transitions to all final states in ^{7}Li below ∿12 MeV and in ^{6}Li below ∿6 MeV are indicated.

Fig. 10. An energy spectrum from the $^{9}Be(\alpha,^{8}Be)^{5}He$ reaction at $\theta_{lab} = 24°$ and E_α = 65 MeV. The locations of possible transitions to all final states in ^{5}He below ∿17 MeV excitation are indicated.

Fig. 11. Angular distributions of the $^{12}C(\alpha,^{8}Be)^{8}Be$ (g.s.) reaction between E_α = 63.2 and 67.3 MeV (a) and of the $^{16}O(\alpha,^{8}Be)^{12}C$ (g.s.) reaction between E_α = 55 and 72.5 MeV. The angular width of each data point is ∿1° and a statistical error bar is shown if it exceeds the size of the data point.

Fig. 12. Absolute experimental (symbols) and calculated (solid curves) $(\alpha,^{8}Be)$ cross sections at E_α = 65 MeV for transitions populating the ^{12}C (g.s.) and several excited states. In this figure and the following ones containing experimental angular distributions, a statistical error is given if it exceeds the height of the data point. In addition, the width of each data point corresponds to the angular acceptance of the ^{8}Be identifier used in measuring that point.

Fig. 13. Absolute experimental (symbols) and theoretical (solid curves) $(\alpha,^{8}Be)$ cross sections at E_α = 72.5 MeV for transitions populating the ^{11}B (g.s.) and three excited states.

Fig. 14. Absolute experimental (symbols) and theoretical (solid curves) $(\alpha,^{8}Be)$ cross sections at E_α = 72.5 MeV for transitions populating the ^{10}B (g.s.) and four excited states.

Fig. 15 Absolute experimental (symbols) and theoretical (solid curves) $(\alpha,^{8}Be)$ cross sections at E_α = 65 MeV for transitions populating the ^{8}Be (g.s.) and first excited state plus the ^{9}Be (g.s.) and an excited state.

Fig. 16. An illustration for the $^{10}B(\alpha,^{8}Be)^{6}Li$ (g.s.) and $^{11}B(\alpha,^{8}Be)^{7}Li$ (g.s.) reactions at 72.5 MeV of the relative contributions of different L-values to the theoretical cross sections (Rotter's[8] values of S^L were used). The theoretical curves for each L value are labelled and the sum of the contributions of both possible L values is given by the solid lines (see text).

Fig. 17. Experimental (symbols) and theoretical (solid curves) (α, ^{8}Be) cross sections at E_α = 65 MeV (^{9}Be and ^{11}B) and at E_α = 72.5 MeV(^{10}B) for transitions populating (a) the ^{5}He (g.s.); (b) the ^{6}Li (g.s.) and 2.18 MeV state and (c) the ^{7}Li (g.s.) and 4.63 MeV state (see text). These theoretical cross sections were calculated with S_α from both Kurath[9] (solid lines) and Rotter[8] (dashed lines).

Fig. 18. (a) A comparison of the ratios of experimental to Kurath's[9] theoretical spectroscopic factors ($R^{abs} \equiv S(exp)/S(theory)$). (b) A comparison of these ratios relative to the ground state ratio for each target (see discussion in text). Note that the ratio (R^{rel}) of S_α relative to the 2.2 MeV state in ^{6}Li is given for $^{10}B \rightarrow {}^{6}Li + \alpha$. In both parts (a) and (b), the ^{6}Li(g.s.) point is off-scale because of its very small theoretical S_α (see Tables V and VI).

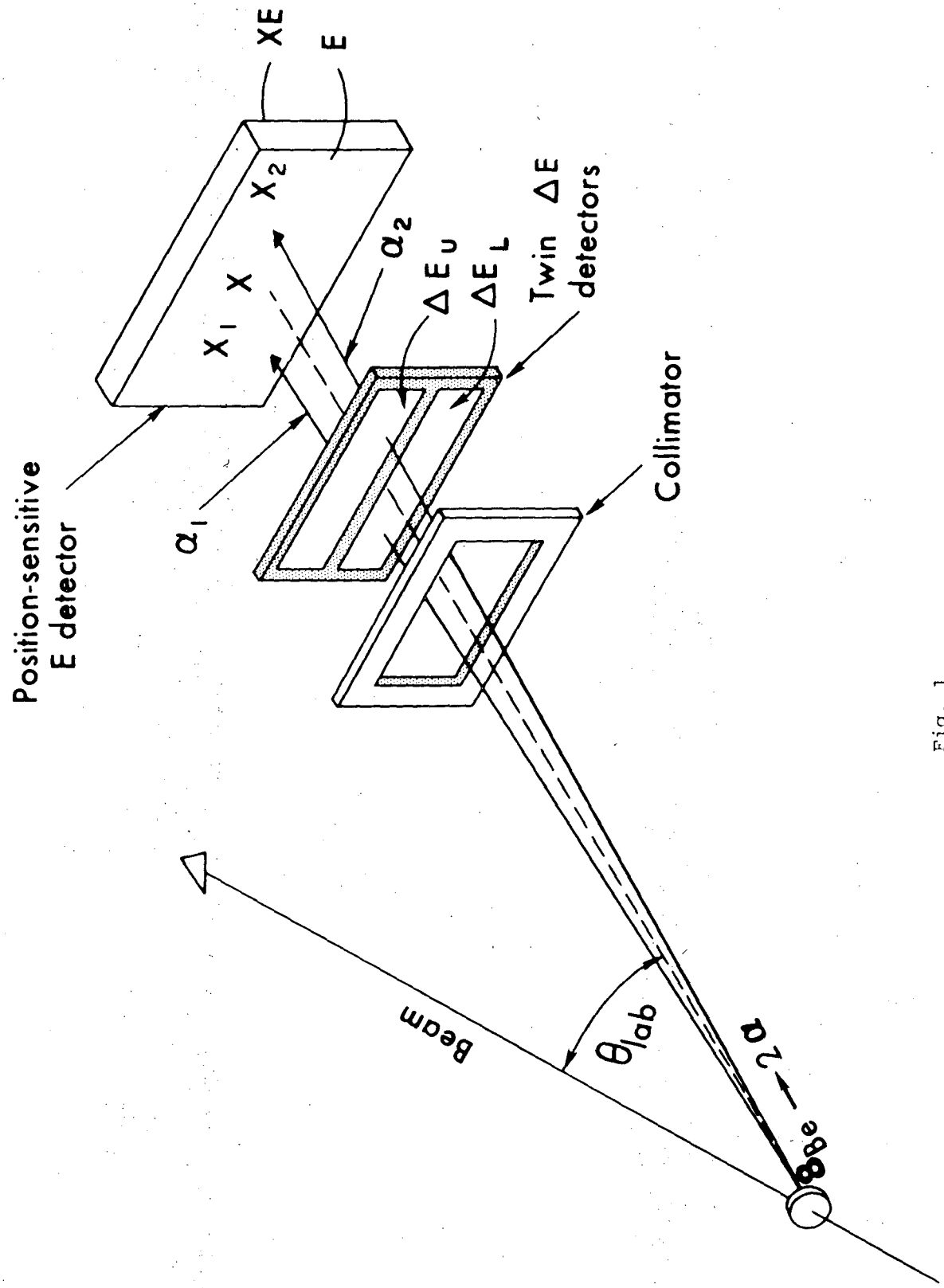

XBL7511-8675

Fig. 1

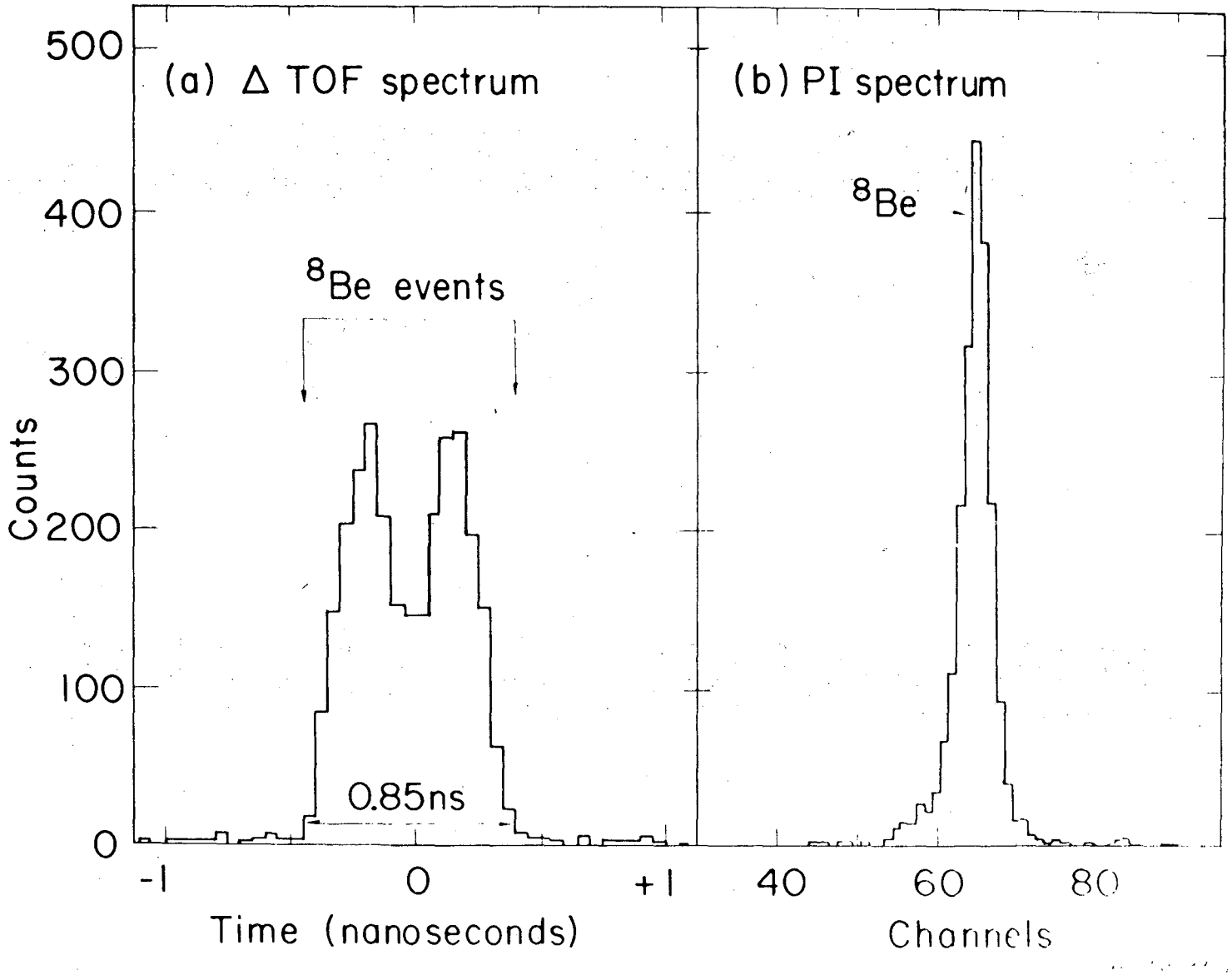
(a) Δ TOF spectrum
(b) PI spectrum
^{8}Be events
^{8}Be
0.85ns
Counts
Time (nanoseconds)
Channels
500
400
300
200
100
0
-1
0
+1
40
60
80

Fig. 2

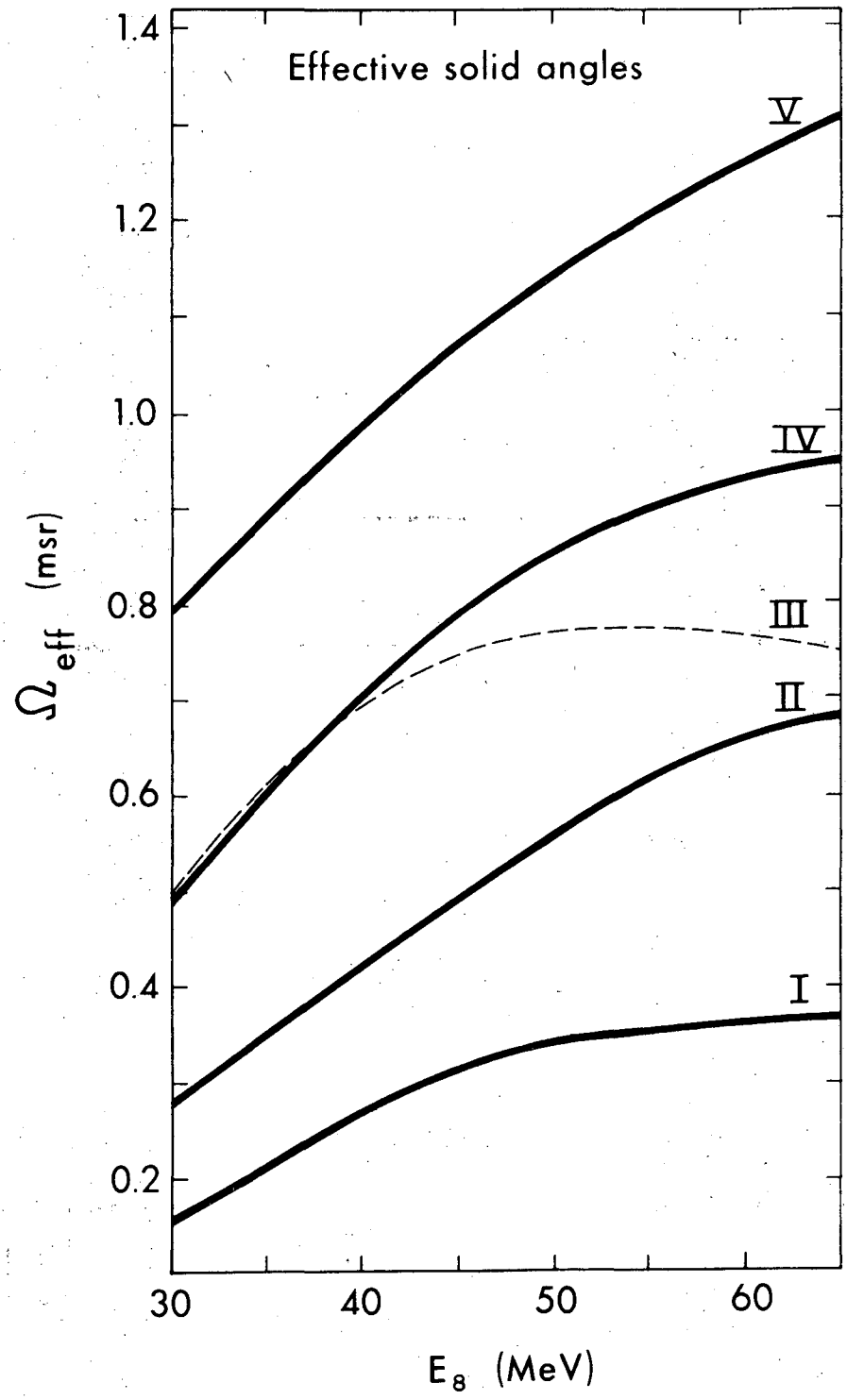

XBL7511-8673

Fig. 3

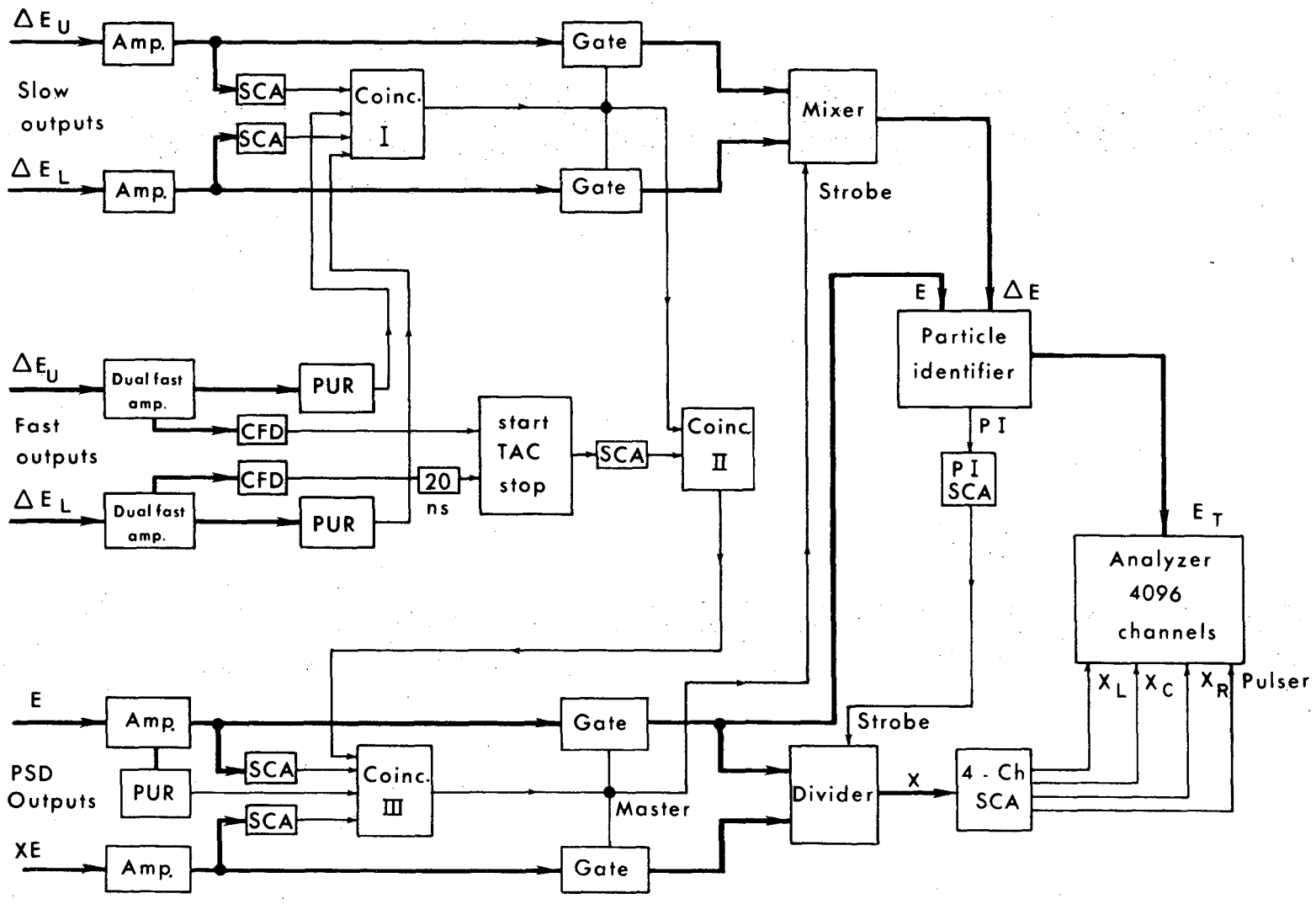

Fig. 4

XBL 7511 - 8674

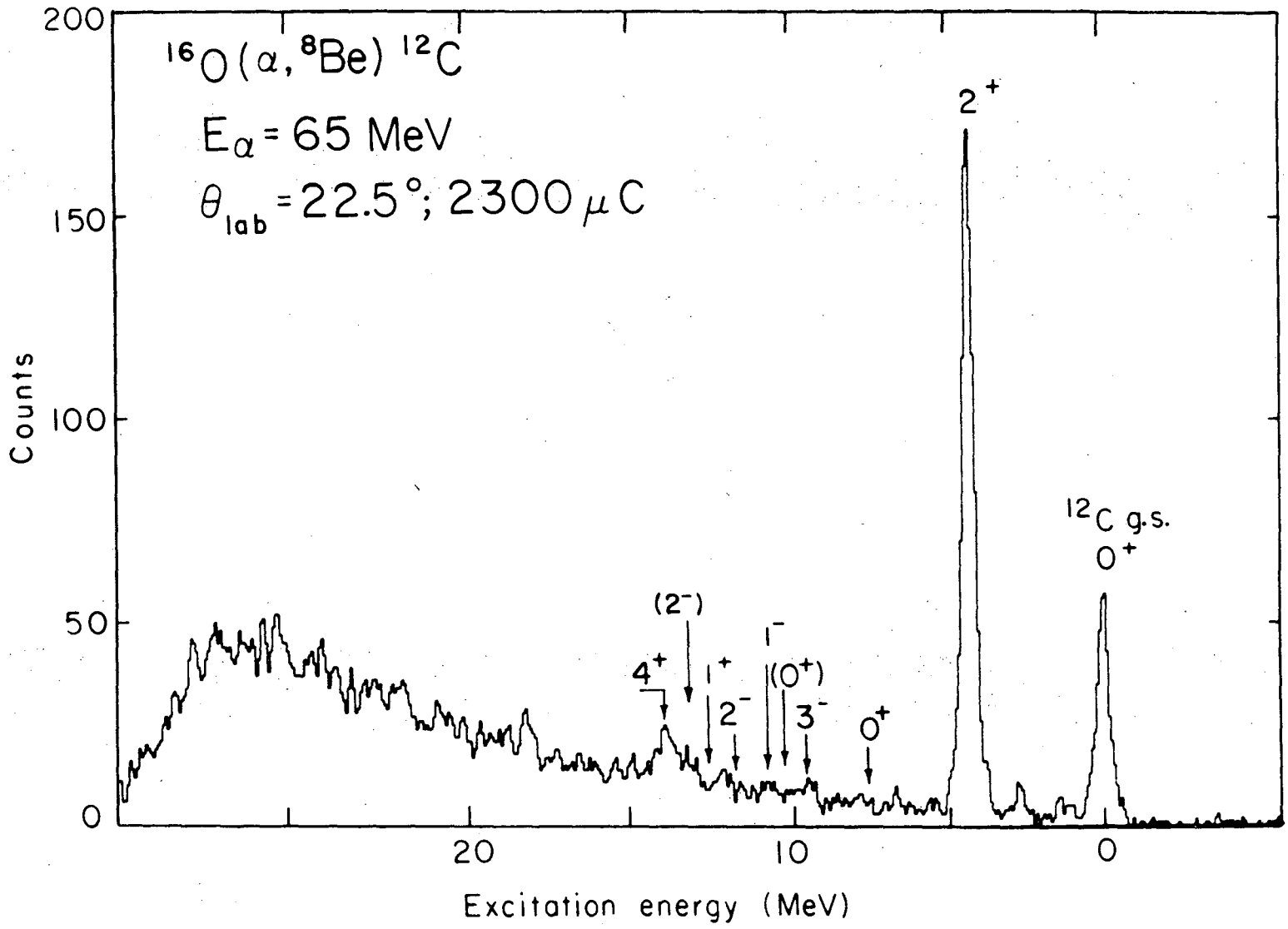

Fig. 5

XBL751-2152

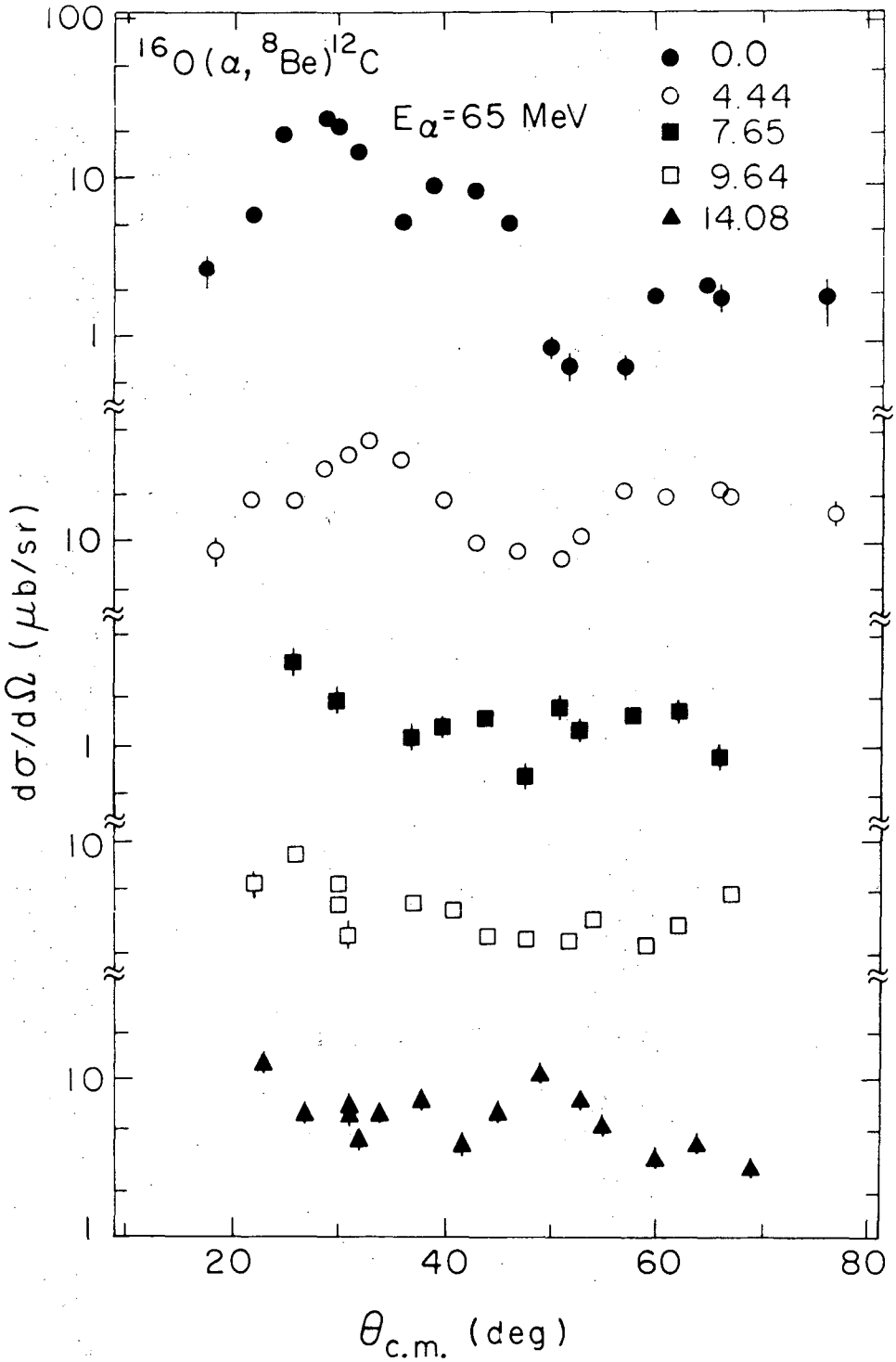

Fig. 6

XBL 7511-8666

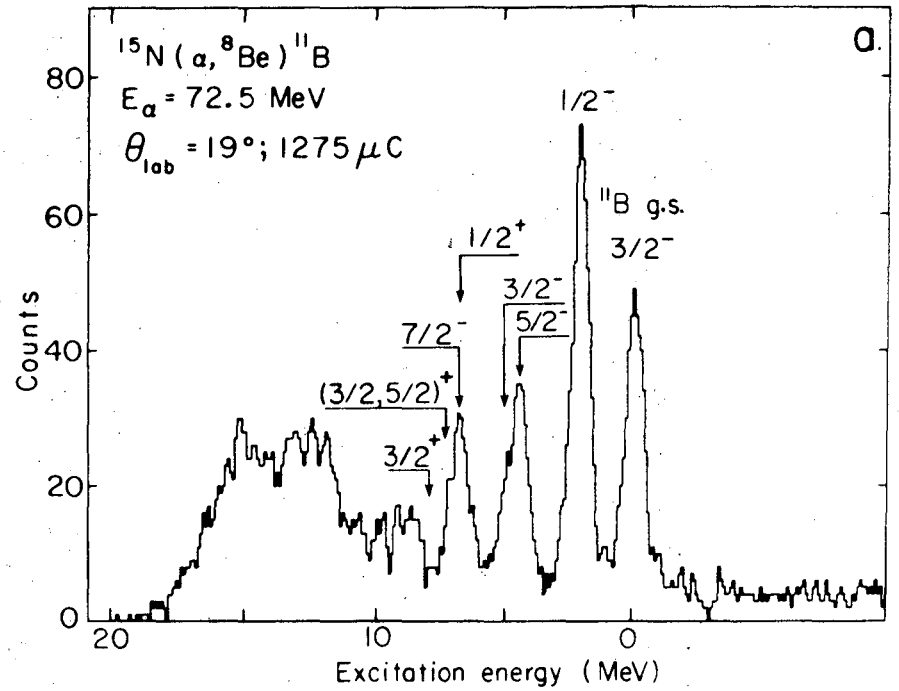

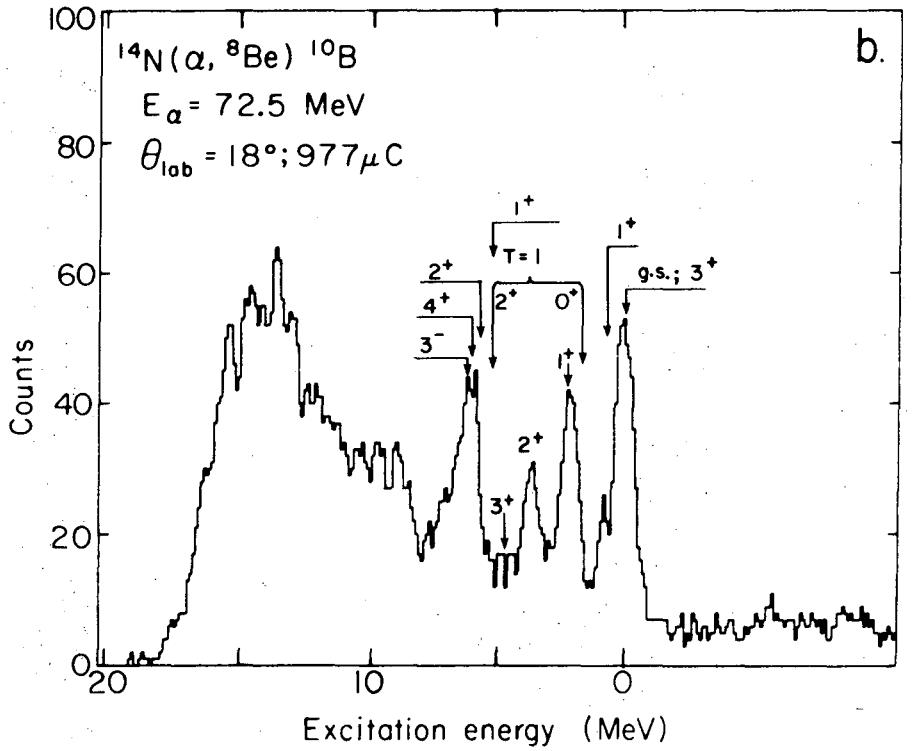

Fig. 7

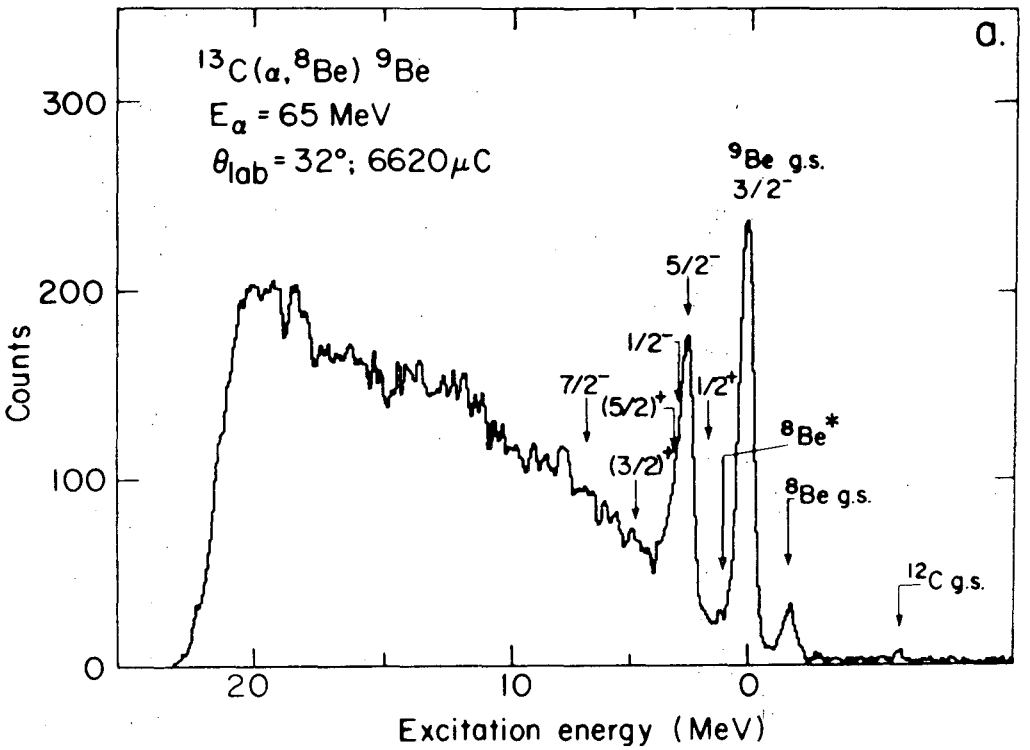
a.
$^{13}C(\alpha,^{8}Be)\ ^{9}Be$
E_α = 65 MeV
θ_{lab} = 32°; 6620μC
^{9}Be g.s.
3/2⁻
5/2⁻
1/2⁻
7/2⁻
(5/2)⁺
1/2⁺
^{8}Be*
(3/2)⁻
^{8}Be g.s.
^{12}C g.s.
Counts
300
200
100
0
20
10
0
Excitation energy (MeV)

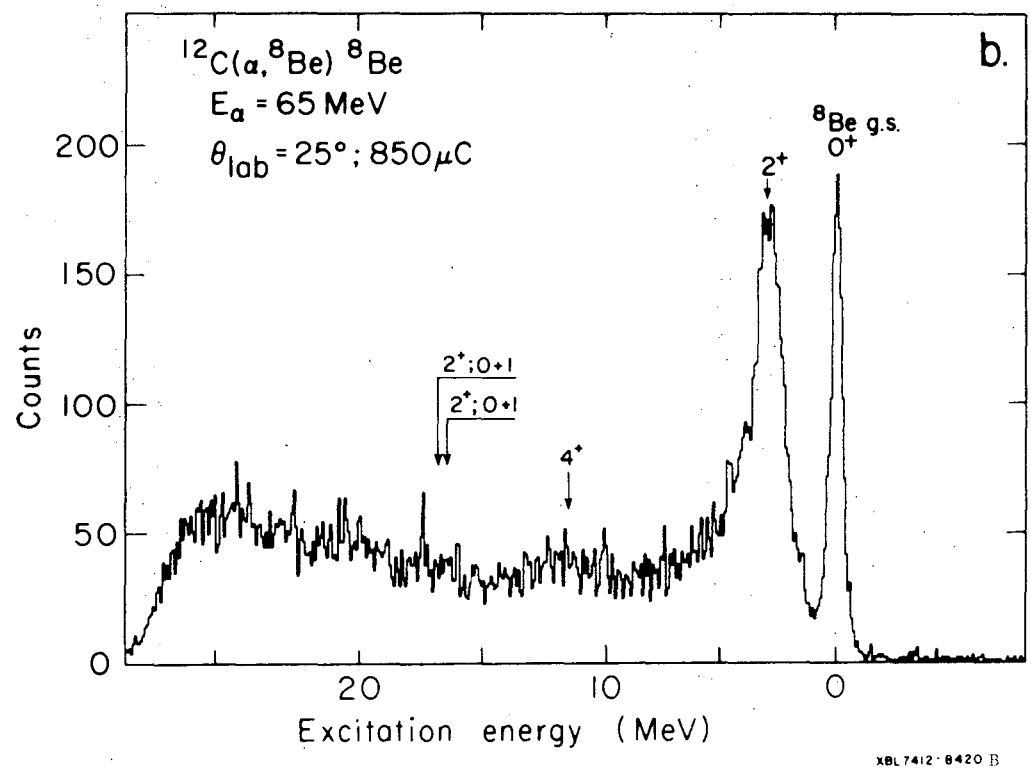
b.
$^{12}C(\alpha,^{8}Be)\ ^{8}Be$
E_α = 65 MeV
θ_{lab} = 25°; 850μC
^{8}Be g.s.
0⁺
2⁺
2⁺;0+1
2⁺;0+1
4⁺
Counts
200
150
100
50
0
20
10
0
Excitation energy (MeV)
XBL7412-8420 B

Fig. 8

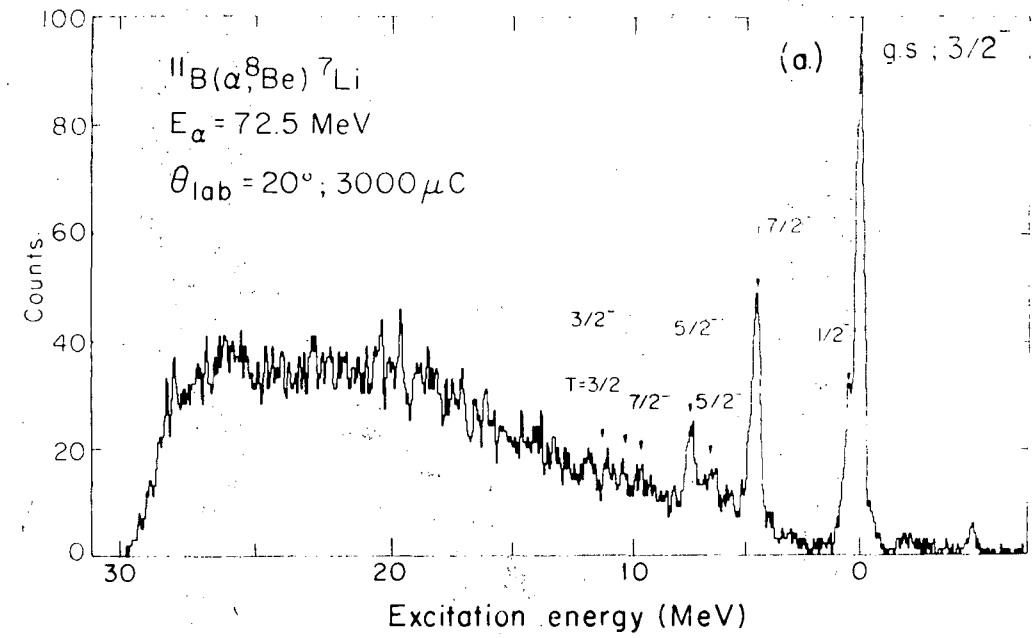

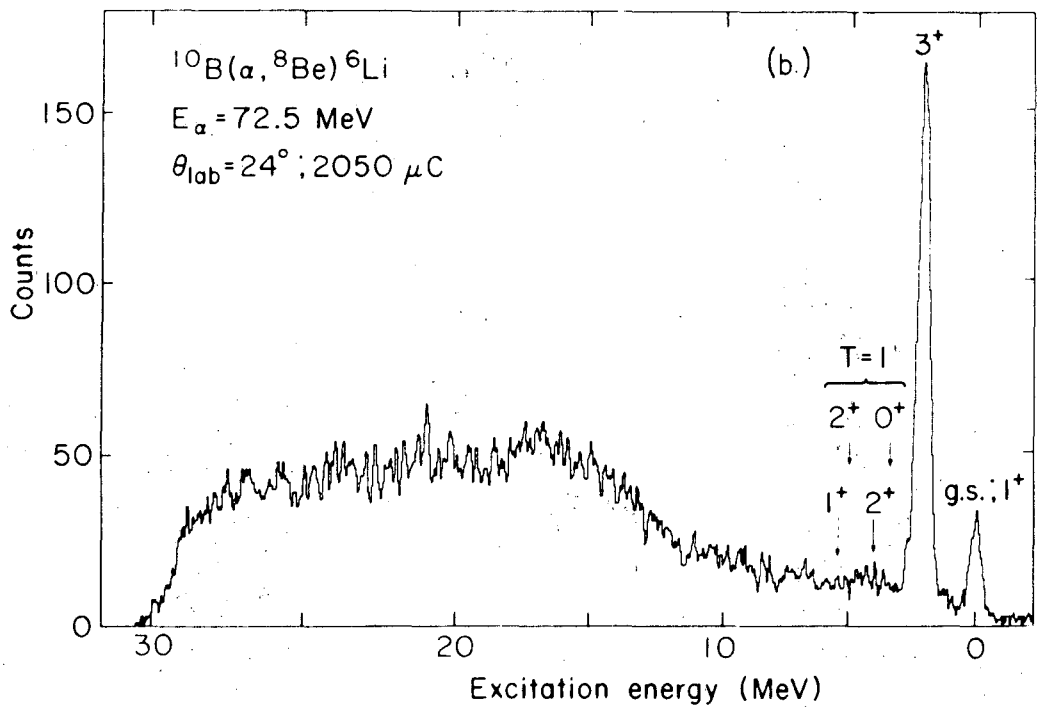

Fig. 9

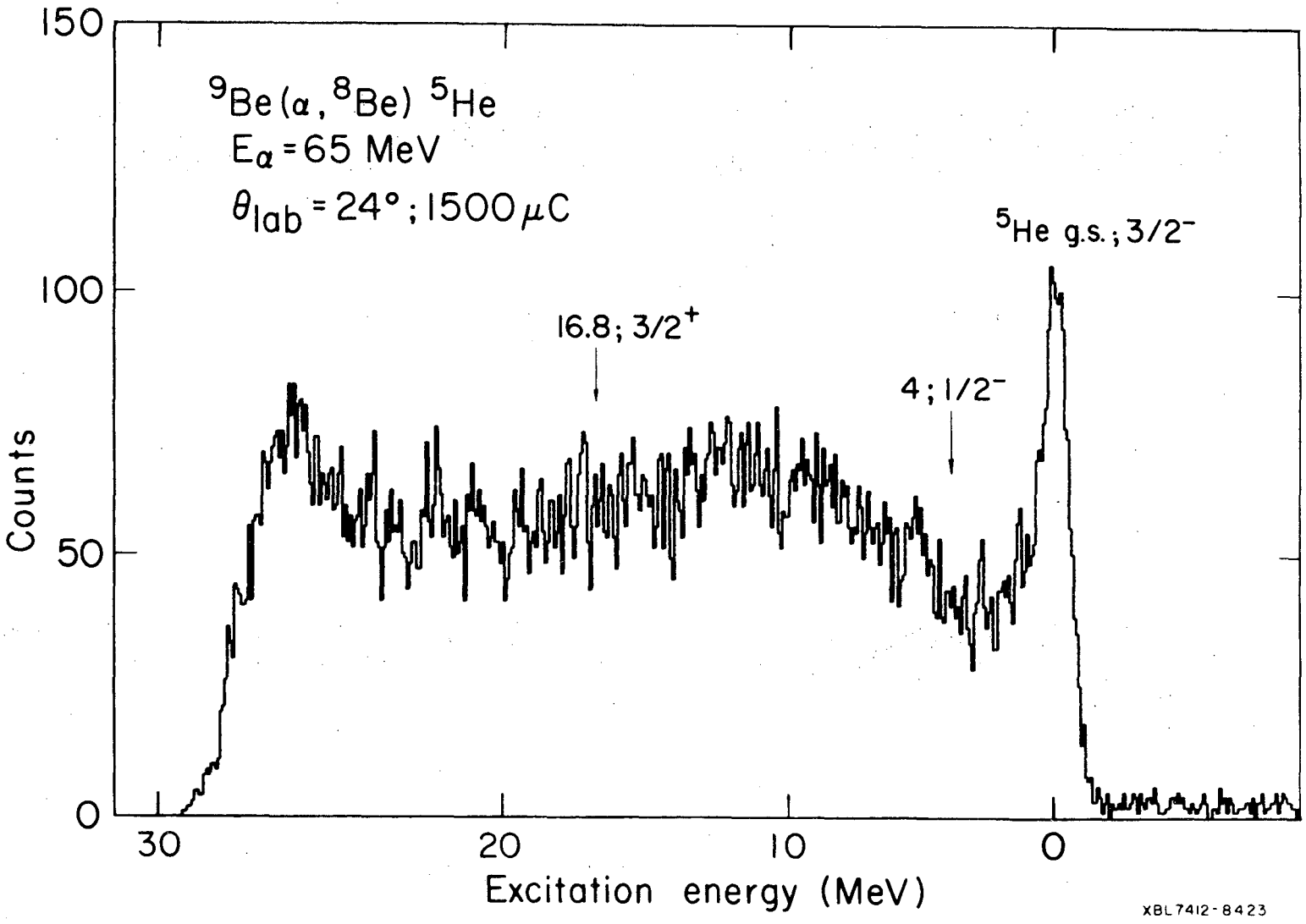
150
100
50
0
Counts
$^{9}Be(\alpha, ^{8}Be)\ ^{5}He$
$E_\alpha = 65$ MeV
$\theta_{lab} = 24°$; 1500 μC
^{5}He g.s.; $3/2^-$
16.8; $3/2^+$
4; $1/2^-$
30
20
10
0
Excitation energy (MeV)
XBL7412-8423

Fig. 10

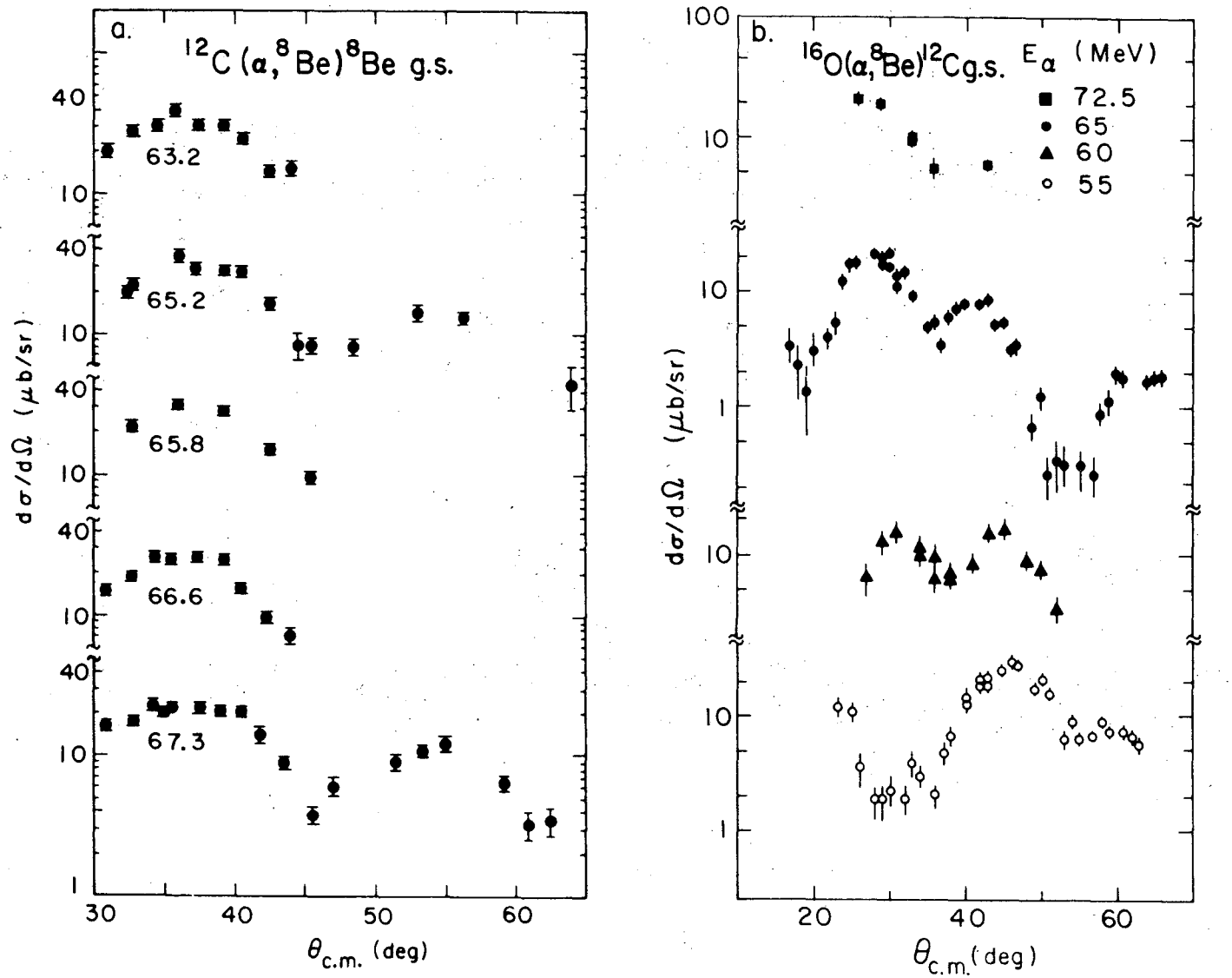
a.
$^{12}C(\alpha,^{8}Be)^{8}Be$ g.s.
63.2
65.2
65.8
66.6
67.3
$d\sigma/d\Omega$ (μb/sr)
$\theta_{c.m.}$ (deg)
b.
$^{16}O(\alpha,^{8}Be)^{12}C$g.s.
E_α (MeV)
72.5
65
60
55
$d\sigma/d\Omega$ (μb/sr)
$\theta_{c.m.}$ (deg)
XBL7511-8667B

Fig. 11

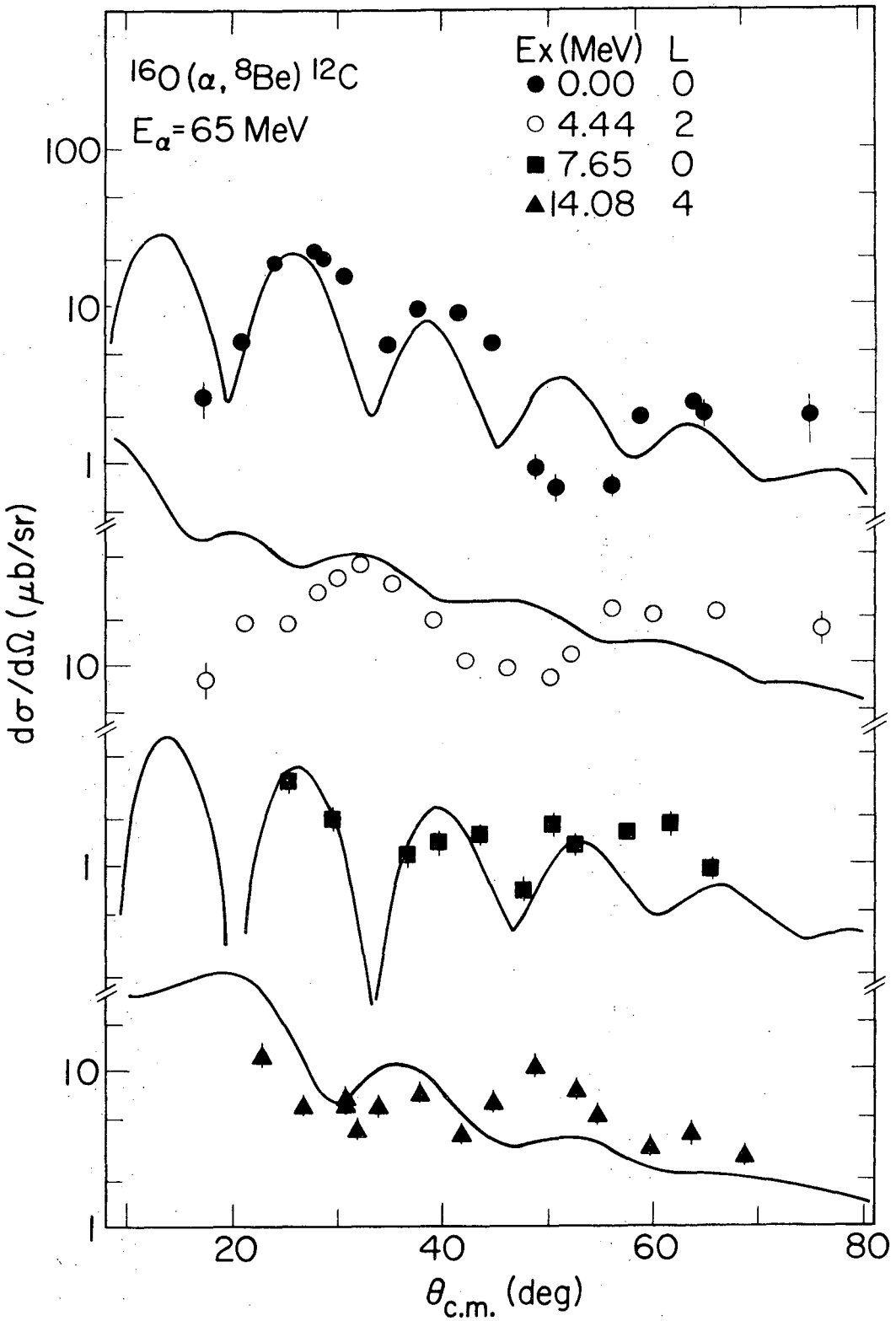
$^{16}O(\alpha, ^{8}Be)\,^{12}C$
E_α=65 MeV
Ex (MeV) L
● 0.00 0
○ 4.44 2
■ 7.65 0
▲ 14.08 4
100
10
1
10
1
10
1
$d\sigma/d\Omega$ (μb/sr)
20
40
60
80
$\theta_{c.m.}$ (deg)
XBL 7512-9930

Fig. 12

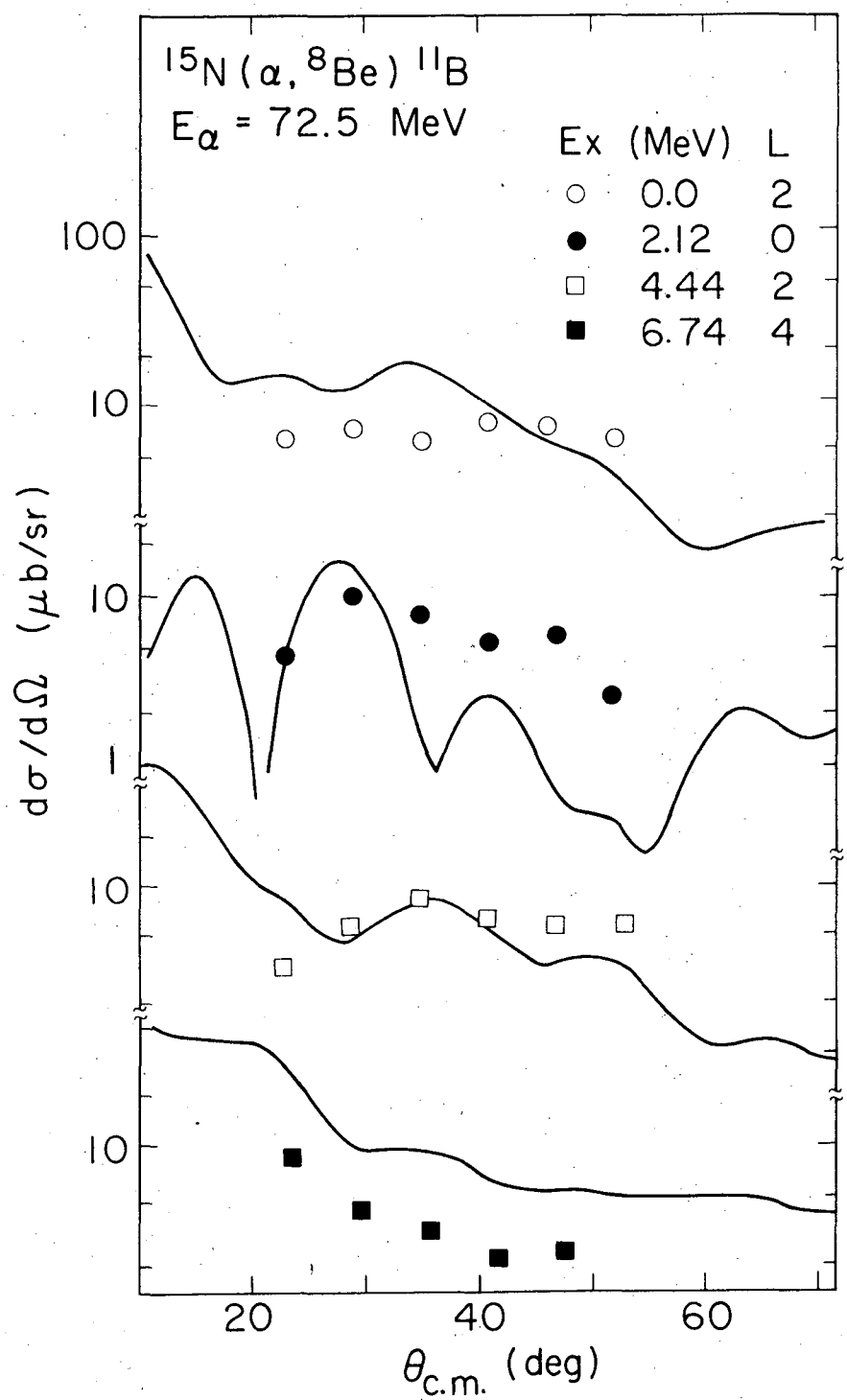

Fig. 13

XBL7512-9928

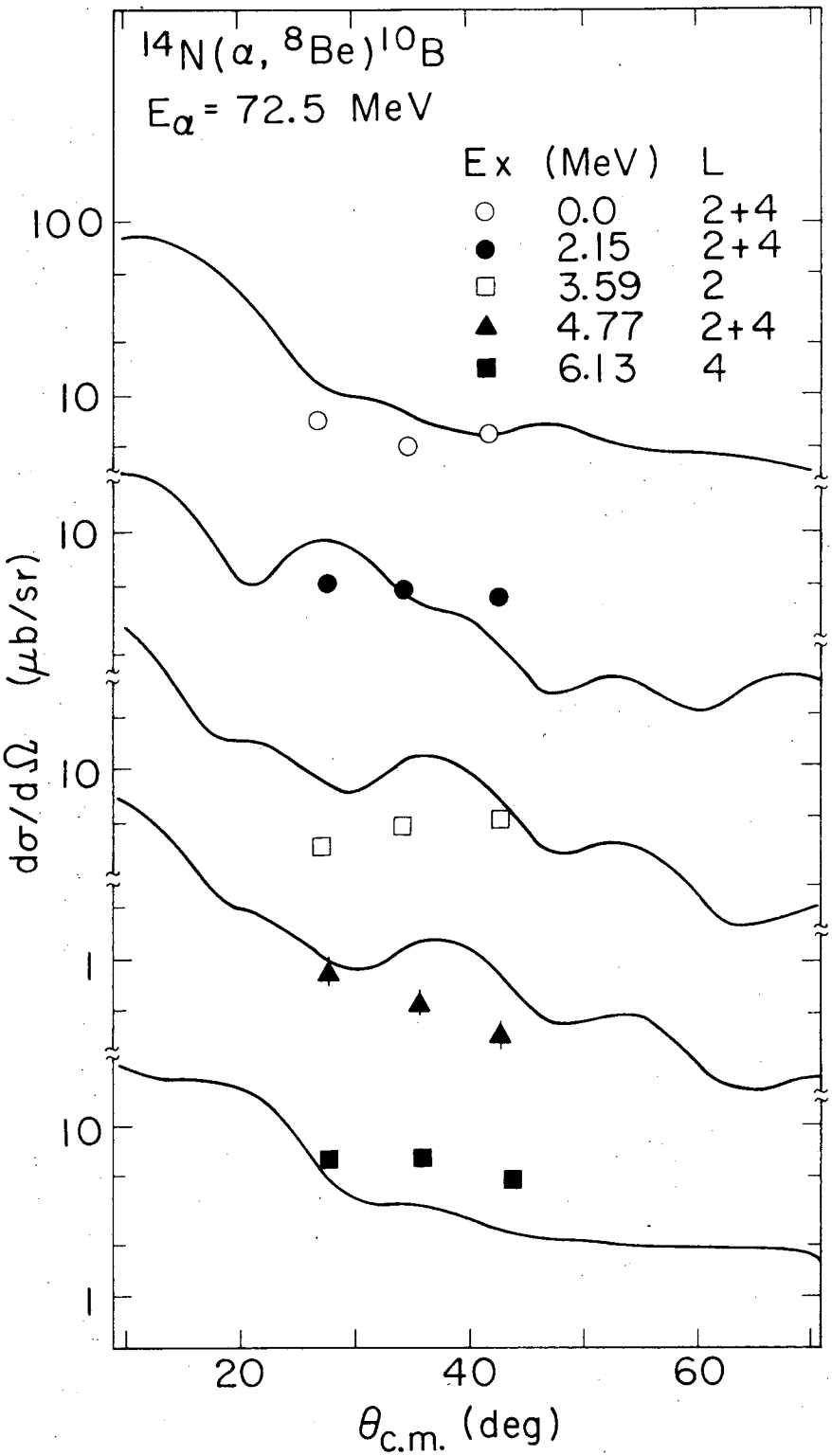

Fig. 14 XBL7512-9927

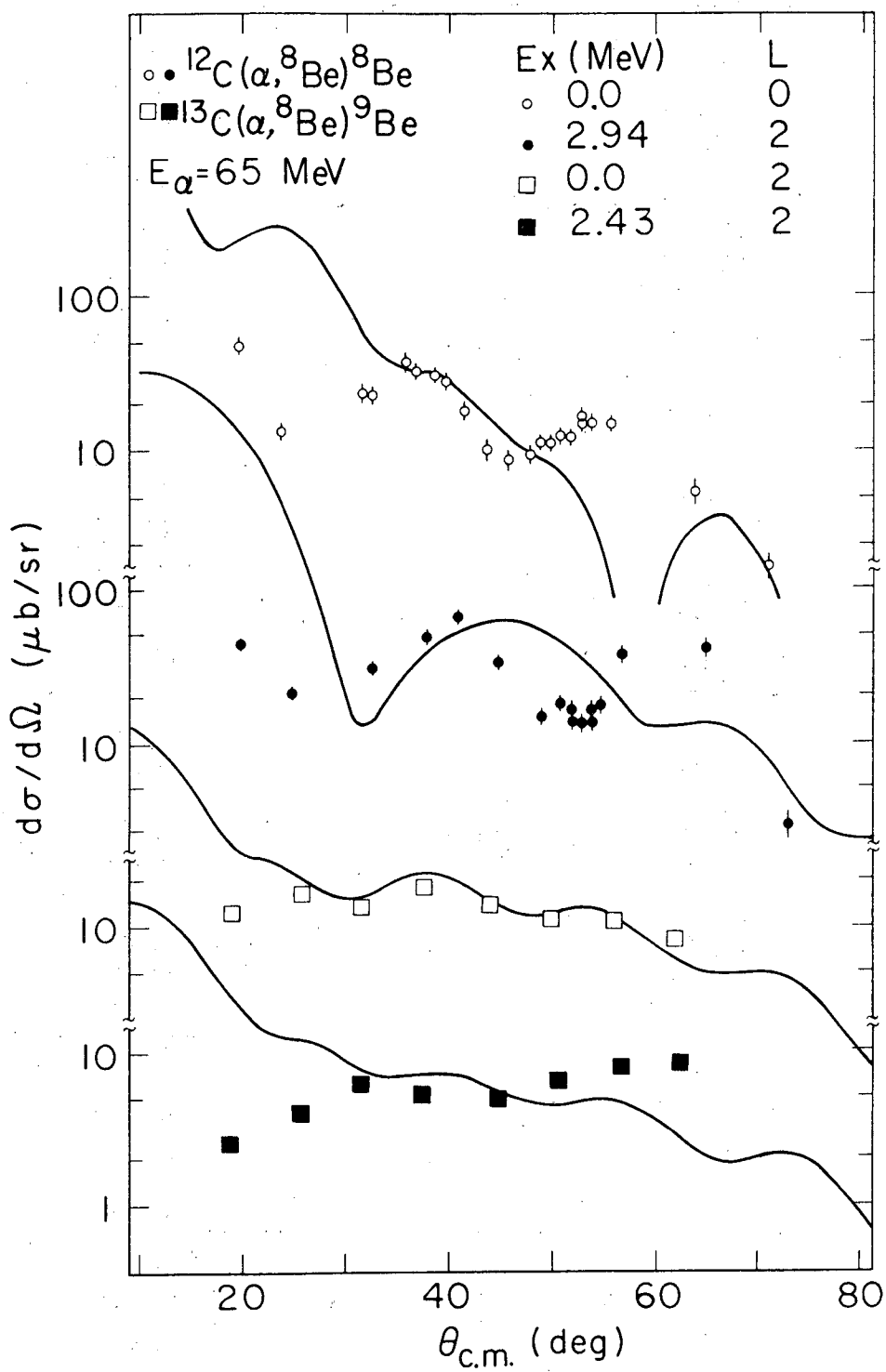

Fig. 15

XBL7512-9929

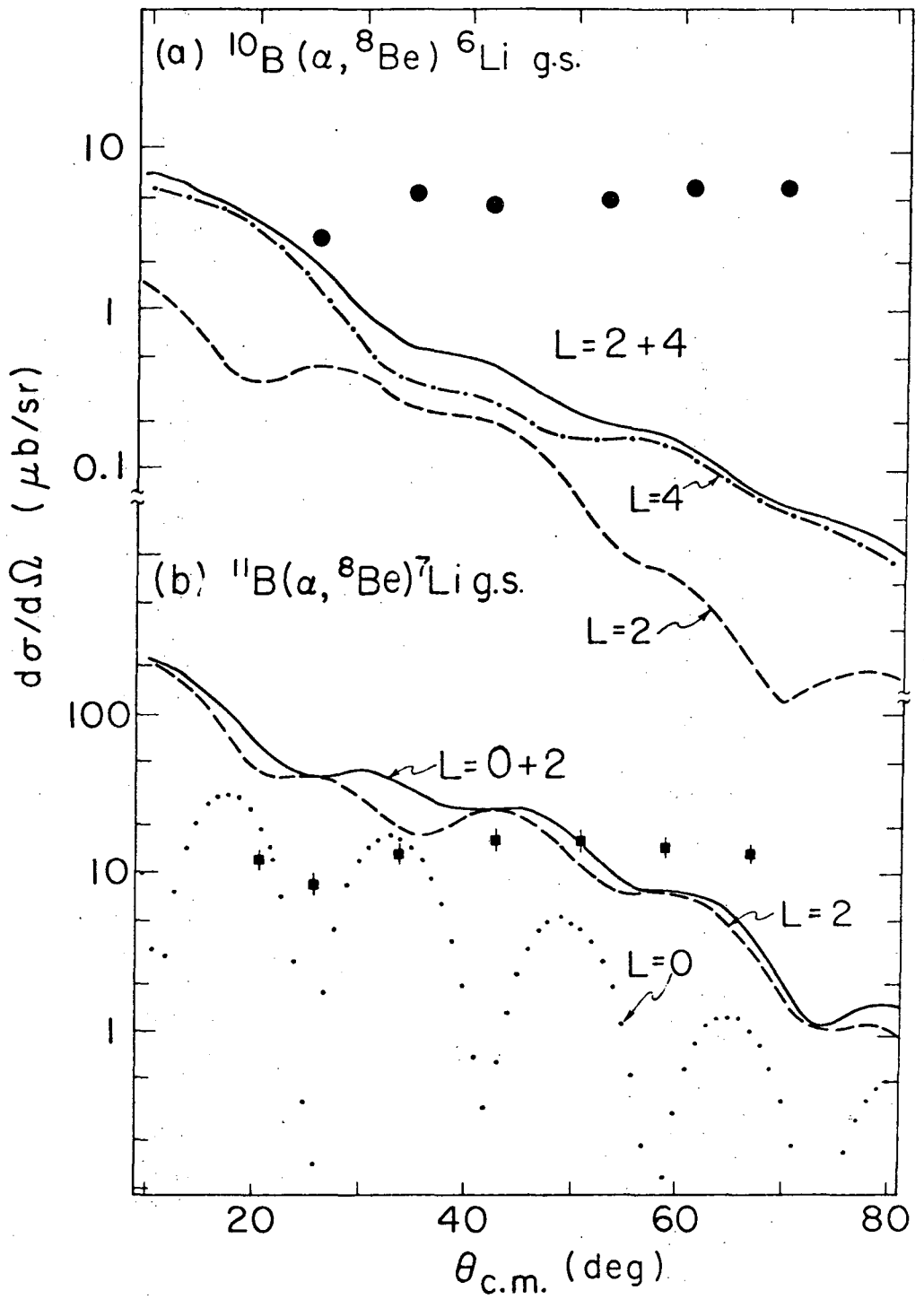

Fig. 16

XBL7512-9925

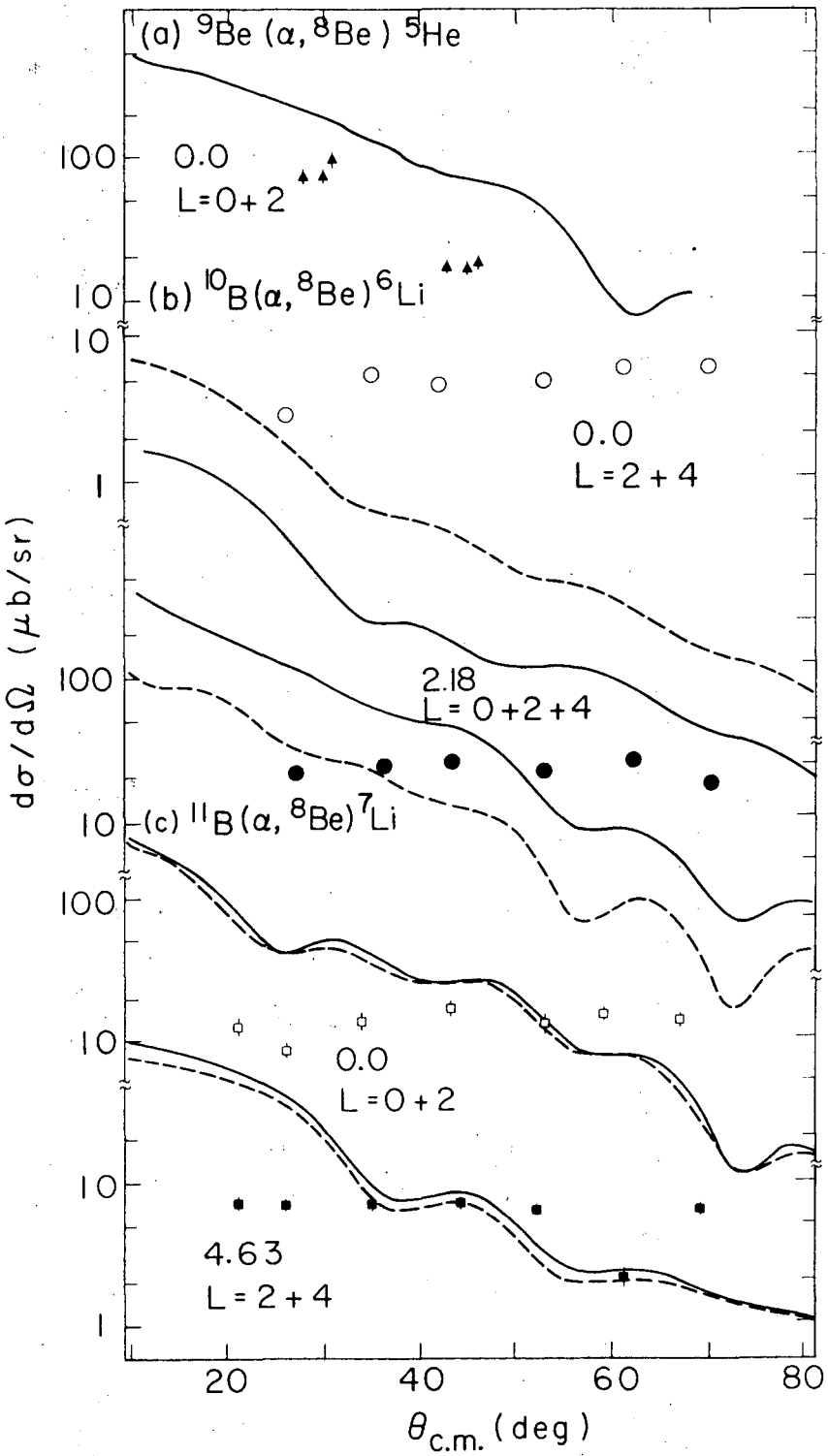

Fig. 17

XBL7512-9923A

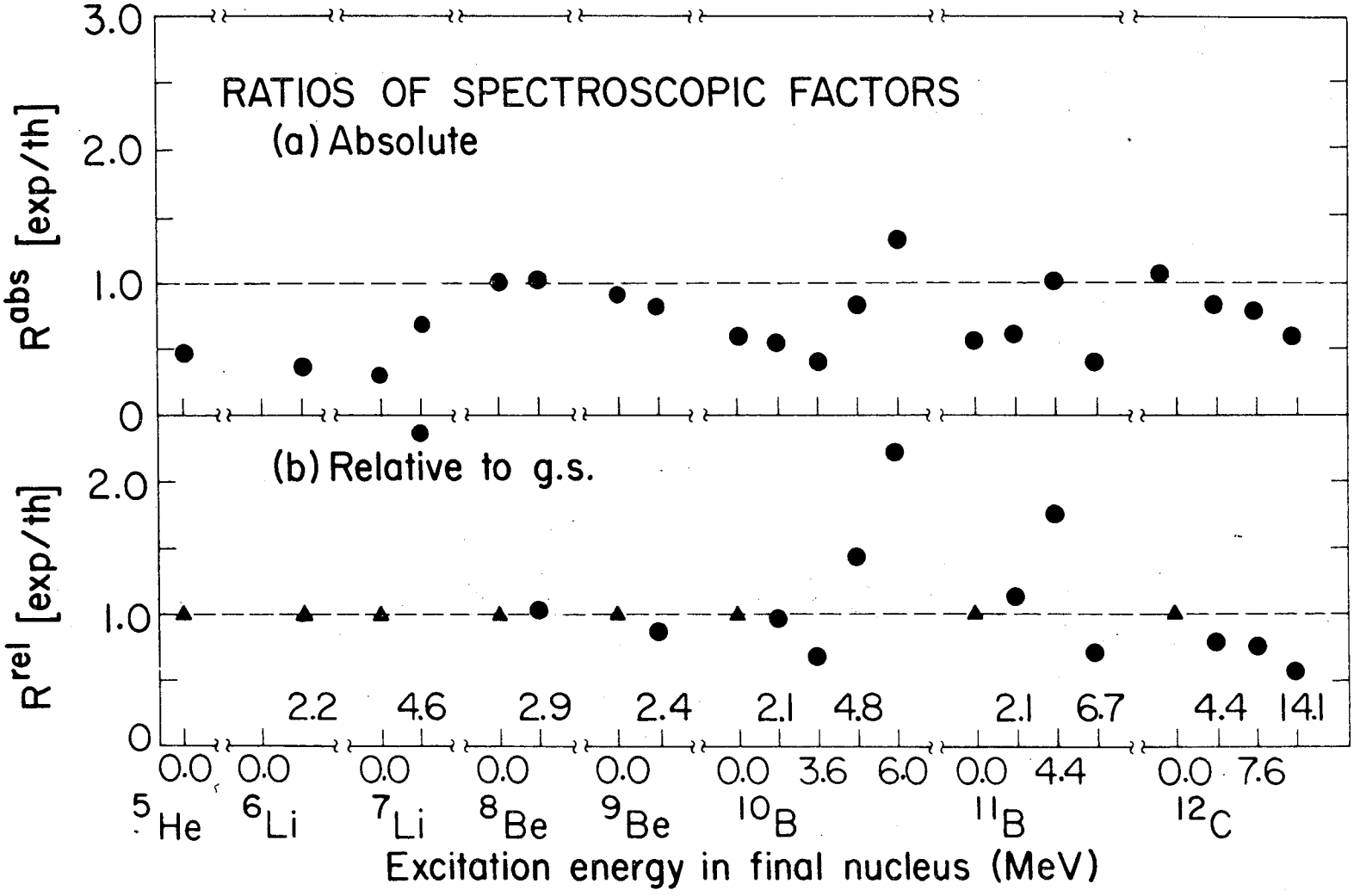

Fig. 18

XBL 7512-9926

TECHNICAL INFORMATION DIVISION
LAWRENCE BERKELEY LABORATORY
UNIVERSITY OF CALIFORNIA
BERKELEY, CALIFORNIA 94720